Research Article

Zukhra Abbasi, Bushra Uzair*, Barkat Ali Khan, Farid Menaa, Mohd Saeed, Irfan Ahmad, and Amjad Islam Aqib*

Tracking success of interaction of greensynthesized Carbopol nanoemulgel (neomycindecorated Ag/ZnO nanocomposite) with woundbased MDR bacteria

https://doi.org/10.1515/ntrev-2024-0027 received January 4, 2024; accepted April 14, 2024

Abstract: Multidrug-resistant wound infections are a global health threat and a leading cause of death, persisting despite available treatments due to antibiotic resistance, biofilms, and ineffective drug delivery systems. The aim of this study is to (i) formulate an innovative nano-drug delivery system (NDDS) based on a Carbopol nanoemulgel (NEG) co-loaded with neomycin-silver/zinc oxide nanocomposite (NC) that could fight clinical MDR and treat biofilm-forming wound pathogens through topical application, and (ii) assess its in vivo woundhealing potential. The silver/zinc oxide (Ag/ZnO) NC was synthesized by co-inoculating the metabolites of Aspergillus welwitschiae and Meyerozyma guilliermondii. The synthesized NC was then conjugated with neomycin and loaded into a Carbopol NEG for efficient topical delivery. The resulting Neo-Ag/ZnO NEG was characterized physicochemically (e.g., UV-visible [UV-Vis] spectrophotometry, field emission scanning electron microscopy, X-ray diffraction, and Fourier transform infrared [FTIR] spectroscopy), biologically (e.g.,

in vitro antimicrobial, antibiofilm, and hemolytic activities), and pharmacologically (e.g., drug content, ex vivo drug release behavior, and in vivo wound-healing potential). The physicochemical analysis confirmed the successful mycosynthesis of the Carbopol NEG-loaded Neo-Ag/ZnO NC. SEM depicted a crystalline polyhedral shape of the small NC (average particle size of 38 nm). FTIR studies showed a slight interaction with the drug and other bioactive moieties in the Carbopol NEG. The Neo content in the Carbopol NEG was as high as 98%, and a maximum release of 81% for Neo, Ag, and ZnO ions was noticed after 12 h. The NDDS appeared hemocompatible and displayed a minimal inhibition concentration of 0.002 µg/mL with the greatest antimicrobial potential against S. aureus (an inhibition zone of 46 mm) compared to other tested wound microbes (p < 0.05). Statistically significant wound-healing activity was found for NDDS (p = 0.0001) in comparison to the control at a concentration of 100 mg/mL. The results showed that this newly developed Carbopol NEGloaded neo-Ag/ZnO NC appeared promising for controlling resistant skin infections and boosting wound regeneration.

Keywords: green synthesis, Carbopol nanoemulgel, Neo-Ag/ZnO nanocomposite, antimicrobial activity, wound healing

Barkat Ali Khan: Drug Delivery and Cosmetics Lab (DDCL), GCPS, Faculty of Pharmacy, Gomal University, Dera Ismail Khan 29050, Pakistan **Farid Menaa:** Department of Internal Medicine and Nanomedicine, California Innovations Corporation, San Diego, CA, 92037, United States of America

Mohd Saeed: Department of Biology, College of Sciences, University of Hail, Hail, Saudi Arabia

Irfan Ahmad: Department of Clinical Laboratory Sciences, College of Applied Medical Sciences, King Khalid University, Abha, Saudi Arabia

Abbreviations

Ag silver
ANOVA analysis of variance

BLAST basic local alignment search tool

B-NEG blank nanoemulgel

CTAB cetyl trimethyl ammonium bromide

DIW deionized water

EDX energy-dispersive X-ray spectroscopy FESEM field-emission scanning electronic

microscopy

^{*} Corresponding author: Bushra Uzair, Department of Biological Sciences, International Islamic University, Islamabad 44000, Pakistan, e-mail: bushra.uzair@iiu.edu.pk

^{*} Corresponding author: Amjad Islam Aqib, Department of Medicine, Cholistan University of Veterinary and Animal Sciences, 63100, Bahawalpur, Pakistan, e-mail: amjadislamaqib@cuvas.edu.pk

Zukhra Abbasi: Department of Biological Sciences, International Islamic University, Islamabad 44000, Pakistan

FTIR Fourier-transformed infrared

(spectroscopy)

ITS internal-transcribed spacer GC-MS gas chromatography-mass

spectrometry

MDR multidrug resistance

MIC minimum inhibition concentration
MRSA methicillin-resistant *Staphylococcus*

aureus

NC nanocomposite
NEG nanoemulgel
Neo neomycin

Neo-Ag/ZnO NEG neomycin-loaded Ag/ZnO NEG
NDDS nano-drug delivery system

NIST National Institute of Standard and

Technology

PBS phosphate buffer solution

PEG polyethylene glycol RBCs red blood cells

RP-HPLC reverse-phase high-pressure liquid

chromatography

UV ultraviolet Vis visible

WTC wound total closure

ZnO zinc oxide

1 Introduction

Untreatable microbial infectious diseases, especially those associated with MDR bacteria, remain the second leading cause of mortality in developing countries and the third leading cause globally, despite several developments in the medical field, as per a 2019 World Health Organization report [1]. Infection is a complication in both acute and chronic wounds. Common resistant pathogens associated with wound infections are *S. aureus, P. aeruginosa*, and *C. albicans* [2]; all three impede the regenerative process, leading to complex amputations and sepsis due to biofilm formation [3,4].

The effectiveness of existing treatments such as Ceftaroline, Fosfomycin, Dalbavancin, and Ceftobiprole against MDR bacteria like methicillin-resistant *Staphylococci aureus* (MRSA), as well as Ceftolozane-Tazobactam, Aztreonam-Avibactam, and Ceftazidime-Avibactam against *P. aeruginosa* is diminishing due to the emergence of resistance mechanisms as stated by Giurazza *et al.* [5]. Likewise, antifungal medications, including fluconazole, chlorhexidine, nystatin, and amphotericin, become less effective as microbes develop resistance mechanisms, which can include the production of enzymes (lipases,

proteinases) [6]. Additionally, the injudicious administration of antibiotics, as highlighted by Ahmed et al. [7], exacerbates the problem, underscoring the urgent demand for innovative antimicrobial approaches [7]. Notably, earlier studies point out the existing gap between the escalating antimicrobial resistance (AMR) and the development of new antibiotics, as elucidated by Pammi et al. [8]. In this context, recent research has shown promising avenues in nanomaterialbased antimicrobials, as bacteria exhibit reduced resistance to metal nanoparticles (NPs) compared to conventional antibiotics [9]. For instance, Ag NPs exhibit broad-spectrum antimicrobial activity, effective against MDR strains [10], but have concerns over cytotoxicity and agglomeration, which can be alleviated by capping Ag with less toxic metal oxide NPs, such as ZnO or polymers [11]. ZnO NPs, approved by the FDA, are widely used in medicine due to their affordability and diverse therapeutic benefits, including anti-inflammatory, antimicrobial, and wound-healing activities [12]. Therefore, Ag-ZnO nanocomposite (NC) could offer a new way of preventing infection and favoring wound healing. In addition, green synthesis methods for metallic NPs have emerged as viable approaches, reducing toxicity and offering significant benefits to the pharmaceutical industry [13]. The fungus-mediated synthesis of metal oxide NPs is novel and more advantageous than synthesis mediated by bacteria or plants [14]. Endophytic fungal strains residing within medicinal plants produce NPs of different sizes, stability, and shapes enhancing their biomedical applications. This is attributed to their ease of handling, ability to produce a large amount of biomass, high metal binding strength, tolerance to metals, and secretion of metabolites [15]. Furthermore, what sets our study apart is the utilization of a fungal consortium for NPs synthesis, which enhances the efficiency and scalability of production while minimizing environmental impact.

The establishment of antibiotic(s) synergism with NPs further enhances the spectrum of antibacterial activity while reducing toxicity by targeted drug delivery [16,17]. Neo (neomycin sulfate), generally recognized as a safe topical antibiotic, acts by disrupting bacterial DNA and protein synthesis, leading to reactive oxygen species (ROS)-induced cell death [18]. Applying this combined approach with Ag/ZnO NC could effectively address wound pathogens resistant to conventional treatments.

Currently, topical DDS are a leading choice for favoring the healing of infected wounds; this increasing interest is due to their high therapeutic index and minimal non-target organ toxicity compared to other routes of drug administration (*e.g.*, systemic [intravenous] and *peroral* [oral]) [19]. Nanoemulgels (NEGs) are the preferred option among topical drug delivery systems (emulsions, gels, or emulgels) for their effective protection of drugs from enzymatic degradation, enhancement

of emulsion stability through increased viscosity, and reduction of surface tension. This results in superior therapeutic efficacy in enhancing drug permeability, bioavailability, and skin diffusion, making NEGs a promising option for topical drug delivery [20-22]. Moreover, these nano-drug delivery systems (NDDSs) provide a controlled and sustained delivery of topical drugs to the targeted site [23]. Recently, a study by Rehman et al. showed the enhanced wound-healing effect of eucalyptol (EU) due to improved permeability and bioavailability provided by the nanocarrier (NEG) [24]. Further, polymeric substances are widely used as matrices in topical formulations, including for wound healing [25–27], to enhance or confer unique properties like stability. In this regard, the synthetic polymer Carbopol is considered safe and widely used as a gelling agent in topical pharmaceutical formulations for sustained release [28]. Hence, the co-delivery of neomycin (topical antibiotic) and green synthesized antimicrobial Ag/ZnO NC using Carbopol NEG (NDDS) would result in a promising in vitro antimicrobial potential against resistant wound pathogens by eradicating biofilm and in vivo wound-healing efficacy due to increased bioavailability, permeability, and sustained release of bioactive moieties at the wound site.

Herein, we aimed to formulate an original Carbopol NEG-loaded Neo-Ag/ZnO NC (Green nanoantibiotic) using a fungal consortium of two strains (i.e., Meyerozyma guilliermondii and Aspergillus welwitschiae), with the hope of enhancing the efficacy to prevent (resistant) infections in wounds and provide a better topical wound healing. The physicochemical characterization, in vitro antimicrobial activity against resistant microbes, and in vivo woundhealing efficacy of the NDDS were also investigated. To the best of our knowledge, this is the first investigation reporting such a promising topical NDDS.

2 Materials and methods

2.1 Chemicals

Cetyl trimethyl ammonium bromide (CTAB), mercaptoethanol, proteinase K, sodium dodecyl sulfate, chloroform, isoamyl alcohol, isopropanol, and triethanol buffer were used for DNA (desoxyribonucleic acid) extraction and purification. Silver nitrate (AgNO₃, 99.9%) and ZnO salts (99.5%) were used to synthesize the NC. Tween 80, polyethylene glycol (PEG) 400, Carbopol 940 (99.99%), and triethanolamine (99.0%) were used to formulate the emulgel. Acetic acid and India ink were used to prepare the fungal stain. All these chemicals were purchased from Sigma Aldrich (St. Louis, MO, USA). Pure (HPLC-grade) neomycin (see datasheet in Suppl. Mat. File) and olive oil

were purchased from the local market. All the reagents used were of analytical grade and did not require further purification.

2.2 Strains

The three microbial strains, i.e., P. aeruginosa, S. aureus, and C. albicans, were isolated from infected wounds of human patients to check their antibacterial and antifungal activity. They were kindly gifted from the National Institute of Health (Islamabad, Pakistan). These skin microbial strains were maintained on their respective growth media at 4°C and were refreshed after 2-3 months.

2.3 Isolation, purification, and genomic identification of fungal strains

Leaf discs of fresh and healthy Madagascar periwinkle and Cupressus plants were prepared. Their surfaces were rinsed with distilled water (dH₂O) and ethanol; subsequently, they were dried before being cultivated on potato dextrose agar plates. Plates were sealed with a sealing film and incubated at 26°C for 4 days. The fungi that grew on the leaf discs were sub-cultured on potato dextrose agar plates several times to obtain a pure isolate (single species); the isolates were then preserved at 4°C [29]. The fungal strains IIUI313 (the purified strain from the Madagascar periwinkle) and IIUI314 (the purified strain from the Cupressus plant), which had rapid growth and large biomass production, were selected to synthesize the NC.

The isolated fungal species were identified phenotypically based on colonial and cellular morphology [30,31], followed by molecular characterization for genotypic identification. A former CTAB method [32] with certain modifications was used to extract the genomic DNA. Nuclear ribosomal internal-transcribed spacers, i.e., forward ITS1 5' TCCGTAGGTGAACCTGCGG-3' (19mer) and reverse ITS4 5'-TCCTCCGCTTATTGATATGC-3' (20mer), obtained from Macrogen (Seoul, South Korea) were amplified using the polymerase chain reaction (PCR) thermal cycler (BIOER, LifeECO, Shanghai, China) in a final reaction volume of 25 µL [32]. The PCR end-product was run on gel electrophoresis (1.5%) at 100 V for 40 min to separate DNA and confirm the amplicon size. The amplified PCR product was sequenced by Macrogen (Seoul, South Korea) using the Sanger sequence technology, and the obtained internal-transcribed spacer-related data of both strains were analyzed using NCBI's (National Center

for Biotechnology Information) BLAST for strain identification [6].

2.3.1 Identification of reducing agents in fungal extracts using GC-MS

Gas chromatography-mass spectrometry (GC-MS QP5050 with a mass detector, Shimadzu, Tokyo, Japan), using helium as the carrier gas, was used for the quantitative analysis of metabolites (including potential reducing and capping agents) in the fungal methanolic extract (20 μ L). The metabolic products present in the fungal extracts (Figures S1 and S2) matched with standard chemical compounds available from the National Institute of Standards and Technology (NIST) 17 library on a mass-spectrum basis [6].

2.4 Mycosynthesis of the Ag/ZnO NC

The Ag/ZnO NC was synthesized using the method described previously [33]. It was modified by mixing cell-free culture extracts from two fungal strains, as shown in Figure 1. Briefly, the NC was prepared by co-inoculation of the fungal extracts M. guilliermondii (IIUI313) and A. welwitschiae (IIUI314). Both species were isolated as endophytes and grown separately in 250 mL of Sabouraud dextrose broth using 500 mL flasks. Flasks with spores were incubated at $25 \pm 2^{\circ}$ C under shaking (120 rpm) for 4 days in dark conditions to produce biomass. This fungal biomass was isolated from the liquid media by physical separation and washed with deionized water (DIW) to remove all unwanted substances. Fresh, clean biomass (24 g) from each strain was placed in two separated 500 mL flasks containing 250 mL of sterile DIW and incubated in a

rotatory shaker under the same previously described conditions. A cell-free filtrate was extracted by filtering the suspension with Whatman filter paper #1. Then, sterile aqueous salt solutions of 20 mL of 1 M AgNO $_3$ and 2 M ZnO were mixed with 50 mL of the fungal extracts (25 mL each), followed by continuous stirring (200 rpm) and heating (40°C) on a magnetic hot plate for 3–4 h. The percentage-to-weight ratio of Ag:Zn was 1:1, and the ratio of salts to extract was 4:5 v/v. The reduction of salts was visualized by the color change and the precipitate formation. A light-brown aggregate at the bottom of the flask was separated by centrifugation at 4,000 rpm, followed by a double washing with sterile dH $_2$ O and a single washing with ethanol to remove all unreacted molecules. The particles were eventually dried, calcined at 400°C, and stored at room temperature (RT) until use.

2.4.1 Conjugation of neomycin drug with Ag/ZnO NC

Conjugation of the antibiotic drug Neo in the synthesized Ag/ZnO NC was adapted from a formerly reported method [34]. Briefly, the NC and Neo solutions were made in dH_2O at a concentration of 0.1 g/mL (w/v) each. The NC solution was then added to the Neo solution, stirred constantly (250 rpm) for 2 h at RT, and incubated for 24 h at RT. After 24 h, the suspension was centrifuged (4,000 rpm) for 20 min at RT to obtain a pellet of Neo-conjugated NC.

2.4.2 Encapsulation efficiency (EE) of neomycin in Aq/ZnO NC

Neo-Ag/ZnO NC was assessed for interactions between NPs and antibiotics using a UV-Vis spectrophotometer

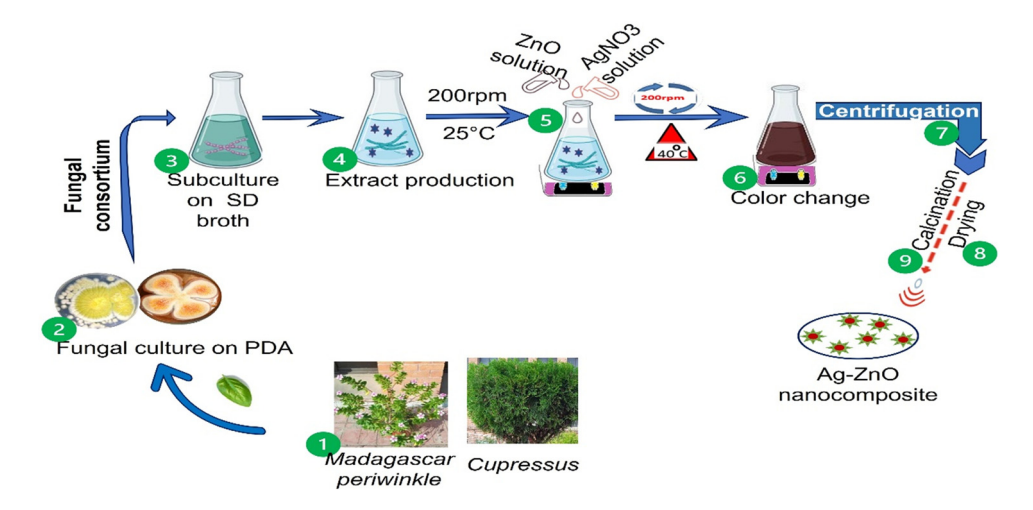


Figure 1: Illustration of the fungal consortium-based synthesis of Ag/ZnO NC.

(HITACHI U 2800, Tokyo, Japan) at the UV-wavelength of 300 nm. The amount of Neo that reacted with the NC was estimated by collecting a volume of supernatant (5 mL) obtained after centrifugation of the neo-conjugated NC and 1/20 dilution in DIW (with 95 mL of DIW). The drug EE was calculated using the following formula [35]:

$$EE(\%) = \frac{Total \text{ amount of drug } - \text{ Amount of free drug}}{\text{Weight of the obtained NPs}} \times 100.$$

2.5 Preparation of NEG formulations

The synthesis of the NEG is a two-step process, which was based on the method published earlier [36]. It was slightly modified by using pure olive oil in the organic phase and drug dissolution in the aqueous phase (Table S1). Three Carbopol NEGs were prepared (Table S2) and named as follows: (i) blank Carbopol NEG, Formulation 1 (blank NEG, F1); (ii) Carbopol NEG-loaded Ag/ZnO NC, Formulation 2 (Ag/ZnO NEG. F2); and (iii) Carbopol NEG-loaded Neo-Ag/ ZnO NC, Formulation 3 (Neo-Ag/ZnO NEG, F3). F3 was selected after optimization using various experimental conditions, as shown in Figure S3.

2.5.1 Step 1. Preparation of nanoemulsions

In this first step, the high-shear homogenization technique was used to mix the organic phase (O) and aqueous phase (W) to synthesize the W/O nanoemulsion. The organic phase was prepared by mixing olive oil and PEG (co-surfactant). Tween 80 (surfactant) was mixed with DIW to prepare an aqueous phase. The NC and the Neo-conjugated NC (50 mg) were added to the aqueous phase and kept in a water bath (GYROMAX 939XL, Amerex Instruments, Inc.) at 70°C for 1h. Subsequently, the oil phase was added in a dropwise manner to the aqueous phase with constant stirring, initially at 800 rpm (low speed) with an electric stirrer for 8 min to avoid surfactant dissociation. As the formulations cooled to RT, the stirrer speed increased to 1,600 rpm (middle speed) for 8 min. Then, the speed of the stirrer was reduced again to low speed to obtain uniform and homogenized emulsions. In the end, the emulsion was exposed to high-shear homogenization (Daihan Scientific, Wonju, Kangwon-do, South Korea) at 10,000 rpm for 10 min to obtain a clear isotropic nanoemulsion.

2.5.2 Step 2. Preparation of gelling solutions

In this second step, a gelling solution was prepared by dispersing 1 g of Carbopol 940 in 99 g of dH₂O (w/w). This was followed by electrical stirring (WiseStir Direct Driven HS-120A, Witeg Labortechnik GmbH, Wertheim, Germany) to obtain a homogenized gel matrix. The gel solution was kept overnight to stabilize it and before its incorporation into the W/O nanoemulsion formulation. Eventually, the nanoemulsion was dispersed (uniformly) into the Carbopol gel matrix at a ratio of 1:1 with constant stirring for 24 min. The whole formulation was subjected to high-shear homogenization at 10,000 rpm to obtain the NEG, as illustrated in Figure S4.

2.6 Physicochemical characterization of the mycosynthesized nanoformulations

2.6.1 Physical analyses

UV-Vis spectrophotometry, field emission scanning electron microscopy (FESEM), X-ray diffraction (XRD), and Fouriertransform infrared (FTIR) spectroscopy were used as the routine state-of-the-art techniques for the physical characterizations of nanoformulations [37]. UV-Vis spectrophotometry (HITACHI U2800, Tokyo, Japan) in a wavelength range of 200-800 nm was used to obtain the spectrum of each NC. The synthesis of NEG was confirmed by DLS using a zeta sizer (Nano ZS 90, Malvern instruments, UK) [38]. FTIR spectroscopy (Tensor 27 MRS, Bruker, Bremen, Germany) was used for infrared spectral analyses of the NEGs, mainly the characterization of their active functional groups and interactions. FESEM (TESCAN MIRA3 XMU, Bremen, Germany) was used to analyze the topography and particle size (PS) of the NCs. Finely grounded NCs were mounted on the microscope stub and Cu-C sputter coated (sputter coater CCU-010 HV, Safematic GmbH, Zizers, Switzerland). FESEM, equipped with an energy-dispersive X-ray (EDX) spectrometer, was also used to analyze the elemental composition of the NEGs. X-ray diffractometry (D8 ADVANCE Bruker, Bremen, Germany) integrated with a LynxEye at 60 kV and 60 Ma allowed to obtain the XRD pattern of dried and grounded NEGs. Information about the phase formation, crystalline morphology, and purity of the NCs were provided. The PS was calculated from the very sharp peak obtained with diffraction analysis by applying the following Debye-Scherrer formula [37,39]:

 $D = 0.9\lambda/\beta \cos \theta$.

2.7 Organoleptic properties

2.7.1 Stability tests

The prepared NEGs (Neo-loaded Ag/ZnO NEG versus blank NEG) were inspected for changes in color, pH, viscosity,

phase separation, odor, and spreadability at 0 h, 24 h, 72 h, 1 week, 2 weeks, and 4 weeks, following methods previously described [27].

2.7.2 Spreadability

The spreadability of the biosynthesized NEGs was determined by using a previously reported slip-and-drag method [27]. Each prepared NEG (2 g) was placed on a stationary glass slide and fixed with an upper movable slide weighing 70 g. The time (in s) taken by the upper slide to cover 8 cm was noted. The same protocol was performed thrice, and the spreadability of the NEG was calculated by the following equation:

$$S = M \times L/T$$

where S was the spreadability, M was the weight (in g) placed on the top slide, L was the length (in cm²) of the glass slides, and T was the time (in s) needed by the upper movable slide to separate from the stationary slide.

2.7.3 In vitro drug release behavior

The release study for the Neo drug, as well as the Ag and ZnO ions from the Neo-Ag/ZnO NEG, was conducted on a Franz diffusion cell apparatus with an artificial cellulose acetate membrane having a pore size of 0.8 µm. The outer jacket temperature was set at 37°C, and the inner compartment was filled with acetate buffer solution (pH 5.5) to mimic in vivo conditions (i.e., human skin pH). One gram of NEG was diluted with 1 mL of acetate buffer and placed in the donor compartment. About 4 mL of aliquot was withdrawn using a sterile syringe from the receptor cell at time intervals of 1, 2, 3, 4, 5, 6, 7, 8, 9, 10, 11, and 12 h, and the receptor cell was then refilled with 4 mL of fresh acetate buffer solution to maintain sink conditions. Samples were collected in test tubes and quantified by measuring their respective absorbance using a UV-Vis spectrophotometer (HITACHI, Model U 2800, Tokyo, Japan) at the UV-wavelength of 280 nm for Neo, 300 nm for ZnO, and 395 nm for Ag. The standard absorbance was found to be 1.250 for Neo, 0.587 for ZnO, and 1.265 for Ag ions. The percentage of nano-antibiotic released from the NEG overtime was calculated using the following formula [36]:

Drug release(%) =
$$\frac{\text{Absorbance of the sample}}{\text{Absorbance of the standard}} \times 100.$$

2.7.4 RP-HPLC determination of neomycin content in the Neo-Ag/ZnO NEG

The amount of Neo in the Neo-Ag/ZnO NEG was quantified using the reversed-phase high-pressure liquid chromatography (RP-HPLC) technique [40] with a C18 column and methanol as the diluent. A standard neomycin sulfate solution and test neomycin solution (analyte) at a concentration of 20 μL were injected separately into the HPLC injection chamber, and the effluents were examined at the UV wavelength of 265 nm. The peak area for the Neo (sample plus standard) was calculated from the calibration curve obtained by analyzing the reaction for 10 min. At a peak retention time of 5.611 min, the Neo content was determined in the conjugate-based NEG. The quantity of Neo in the Neo-Ag/ZnO NEG was calculated using the following equation:

Quantity(%)

$$= \frac{\text{Average area of the sample} \times \text{Claimed quantity}}{\text{Average area of the standard}} \times 100.$$

2.8 Biological and safety characterization of the mycosynthesized Neo-Ag/ZnO NEG

2.8.1 In vitro antimicrobial assays using DDM

The antimicrobial potential of the Neo-Ag/ZnO NEG (50 μg/mL) was screened for the wound infection-causing pathogens S. aureus, P. aeruginosa, and C. albicans, using the disc diffusion method (DDM) in agar-agar [41,42]. Commercially available Neo ointment was used as a positive control and blank disk was used as a negative control. Inoculums from freshly prepared overnight culture strains of S. aureus and P. aeruginosa in nutrient broth and C. albicans in potato dextrose broth having 10⁵ colony-forming units (CFU) were swabbed over solidified agar plates. About 10 μL from a stock solution (50 μg/mL) of Ag/ZnO NC, Neo-Ag/ZnO NC, and Ag/ZnO NEG were also used as internal controls to impregnate discs. All the dried discs were kept on inoculated agar plates and incubated overnight at 37°C to measure the size of the ZI (in mm). The values were calculated thrice, and the results were averaged.

2.8.2 *In vitro* antimicrobial assay by minimal inhibition concentration (MIC)

MIC assay is used to determine the lowest concentration of an antimicrobial agent that prevents the visible growth of a microorganism. The agar-well diffusion method based on a previously published work [43], albeit with a slight modification in the dilution factor, was used to analyze MIC of Neo-Ag/ZnO NEG against MRSA isolated from a wound site of a patient. MRSA suspension was prepared in Mueller-Hinton broth (MHB), and turbidity was visually compared to a 0.5 McFarland standard, followed by swabbing onto a Mueller-Hinton agar plate. About 50 µL of five different dilutions having serial concentrations of 0.16, 0.12, 0.08, 0.04, and 0.02 mg/mL of the prepared NEG formulation was added to each well in the inoculated agar plate. The ZI (mm) around each well following overnight incubation was measured to determine the MIC of the NEG.

2.8.3 Biofilm disruption assay against MRSA

Neo-Ag/ZnO NEG was assessed for its antibiofilm potential against MRSA by biofilm diffusion assay [44]. A suspension of MRSA with an approximate cell density of 1×10^8 CFU/mL was maintained in MHB. An MRSA suspension of 100 µL was added to 10 mL of MHB in a sterilized test tube and incubated for 24 h under static conditions. The biofilm was stained with crystal violet, and the excess stain was rinsed off with dH₂O. This was followed by the addition of a 30% acetic acid solution. In addition to the tube containing cells treated with Neo-Ag/ZnO NEG, the assay also included a negative control in a tube containing only the medium, and a positive control in a tube containing untreated cells. The content from the tubes was analyzed at the Vis-wavelength of 595 nm by spectrophotometry (HITACHI, Model U 2800, Tokyo, Japan).

2.8.4 In vitro hemocompatibility

The in vitro hemolytic studies of the as-synthesized NEG followed the protocol reported in previous studies [45]. A freshly acquired 5% blood sample in an EDTA tube was obtained from a healthy volunteer after written consent (ICF20221011-001) and following the guidelines of the Declaration of Helsinki. The blood was poured into a nutrient agar medium at RT and mixed thoroughly. Neo-Ag/ZnO NEG (200 µL) was transferred to a well and incubated at 37°C for 24 h to evaluate hemolysis. Triton X-100 (positive control, 200 μL), 1× PBS (negative control, 200 µL), and neomycin (standard, 200 µL) were also employed to optimize the experiments.

2.9 In vivo wound-healing potential

2.9.1 Animal selection

White albino mice (6 males and 6 females, N = 12) of 14 weeks with an average weight of 250 g were selected to

evaluate the in vivo wound-healing efficacy. The mice were housed in cages in a well-ventilated area at 25°C and fed ad libitum prior to the experiment [40].

2.9.2 Experimental protocol

The mice were anesthetized with Ketamine HCl injection (50 mg/kg) and shaved. Then, a wound area of 400 mm² was created on the back using a biopsy punch. In the setup experiment, 4 mice (2 males and 2 females) were used as control (untreated group) and 8 mice (4 males and 4 females) were tested with Neo-Ag/ZnO NEG (treated group) to assess its in vivo wound-healing activity. The Neo-Ag/ ZnO NEG (100 mg) was applied to the mouse twice a day for 30 min, and the total wound closure, which is attributable both to contraction and to re-epithelialization [46], was measured at 4-day intervals using the following formula [47]:

$$WTC(\%) = \frac{WA^0 - WA^t}{WA^0} \times 100,$$

where WA⁰ represents the wound area at day 0, and WA^t represents the wound area at time point t.

2.10 Statistical analysis

The one-way ANOVA, repeated measures (RM), one-way ANOVA, and unpaired t-test were performed using Graphpad Prism 8.0.2 (San Diego, CA, USA). Experiments were performed thrice, and the obtained values were presented as mean ± SD. p-values <0.05 were considered as statistically significant.

Ethical considerations: Animal experimentations were approved on 12/27/21 by the ethical review board (ERB) of the International Islamic University, Islamabad, Pakistan (Reg #470-FBAS/MSBT/ F20). The experiments were conducted according to the recommendations and guidance of this ERB. All precautions have been undertaken to minimize the suffering of animals.

3 Results and discussion

With approximately 100 million people suffering from acute wounds and 300 million from chronic wounds worldwide, addressing these conditions poses a substantial economic burden [3,48]. However, despite the availability of various therapeutic wound-healing agents, the challenge of effectively treating infectious wounds persists due to microbial resistance to antibiotics. To overcome this hurdle, metallic NPs have emerged as a promising alternative, as microbes exhibit less resistance to them. Nonetheless, the cytotoxicity associated with metallic NPs could be mitigated by encapsulating them with polymers, thus enhancing their therapeutic potential in wound-healing applications [11]. Hence, current research focused on the production of a new and potent broad-spectrum green nano-antibiotic, namely Neo-Ag/ZnO NEG, to combat MDR wound pathogens while favoring wound healing. Topical antibiotic "neomycin" was incorporated with Ag/ZnO NC to increase its antimicrobial potential. Further, this combination was loaded into NDDS for maximum therapeutic effect on resistant pathogens on wound beds while reducing toxicity. In this pioneered study, a selected fungal consortium produced Ag/ZnO NC in a large amount (4 g) within a short incubation time (3-4 h), which might be due to the secretion of metabolites (including reducing and capping agents) in substantial amounts, as indicated by GC-MS analyses.

3.1 Identification of fungal strains

Morphological features of major fungal strains, respectively, found in *M. periwinkle* and *Cupressus* plant leaves,

were examined. The colonial and cellular morphology revealed with India ink and without India ink (control) is shown in Figure 2; the findings were confirmed by molecular characterization. The IIUI313 strain found in the *M. periwinkle* leaves was *M. guilliermondii* (GenBank accession number: OP216058), and the IIUI314 strain found in the *Cupressus* leaves was *A. welwitschiae* (GenBank accession number: OP216102). A phylogenetic tree of these identified fungal strains was constructed using Mega-7 software by the neighbor-joining method with 700 bootstrap replications, as represented in Figure 3.

3.2 Phytochemical analysis of the mycoextracts by GC-MS

Myriads of metabolic products were detected and analyzed by GC-MS in the extracts of *M. guilliermondii* (Figure S1, Table S3) and *A. welwitschiae* (Figure S2, Table S4). The main chemical compounds found in *M. guilliermondii* were squalene, di (1,2,5-oxadiazolo) [3,4-b:3,4-E] pyrazine, stearic acid, 10(E),12(Z)-conjugated linoleic acid, and dibutyl phthalate, whereas 1,2-benzenedicarboxylic acid, palmitic acid, phthalic acid, stearic

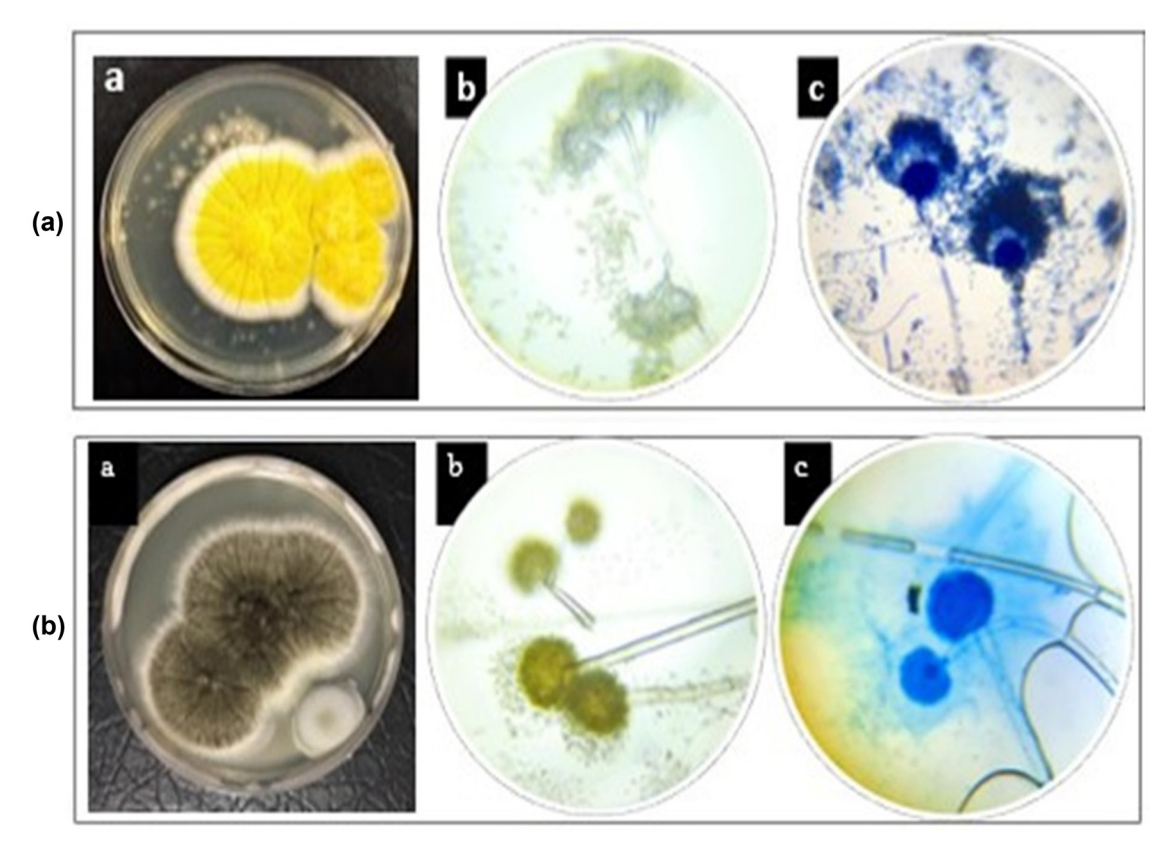
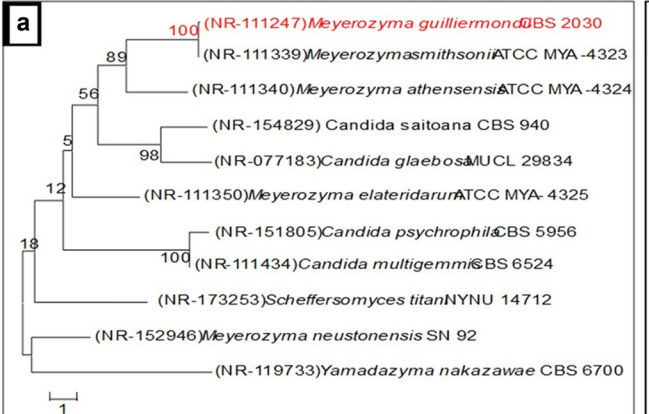


Figure 2: Phenotypic identification by optical microscopy of *M. guilliermondii* (a) and *A. welwitschiae* (b): ((a) colonial morphology; (b) cellular morphology without staining; (c) cellular morphology with India-ink staining. Magnification ×40).



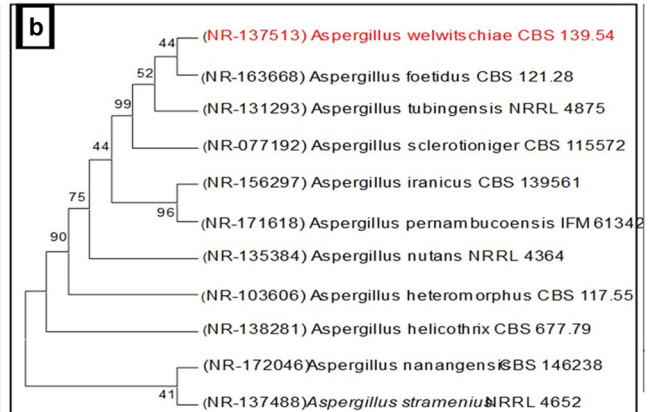


Figure 3: Genotypic identification of M. guilliermondii (a) and A. welwitschiae (b).

acid, 2,2-methylenebis[6-(1,1-dimethylethyl)-4-methyl-phenol were detected in *A. welwitschiae*. These metabolites can not only contribute to the identification of the fungal strain but also, like phytochemicals, might act as reducing and capping agents during the production of NC (*e.g.*, Ag/ZnO NC). Thereby, these metabolites most likely reduced the salts Ag²⁺ to Ag⁰ and Zn²⁺ to Zn⁰ since a color shift was noticed from white to dark brown during the synthesis of Ag/ZnO NC. The selected strains produced a relatively high yield of Ag/ZnO NC (*i.e.*, 4 g) in a relatively short time (within 3–4 h). Moreover, this metabolic diversity enhances the properties of the NPs, including stability and variations in shape. Similar to the varying reducing powers of different agents, as reported by Yoo *et al.* [49], the distinct bioactive compounds and enzymatic activities present in each fungal extract play a crucial role in influencing the synthesis of NPs.

3.3 Physicochemical characterizations of the mycosynthesized nanoformulations

The EE of Neo (100 mg/mL) in Ag/ZnO NC analyzed using a UV-visible spectrophotometer was calculated as 81%. The high encapsulation efficiency of the drug in the Ag/ZnO NC was probably due to the high-level solubility of Neo in the solvent ($\rm H_2O$). The results were compatible with a recent study that reported the encapsulation efficiency of azithromycin to range between 50 and 87% in ZnO NPs using drug concentrations in the range of 200–500 mg [50].

The strong and broad absorbance peaks at 370 nm for ZnO, 410 nm for Ag, and 415 nm for Neo-Ag/ZnO NC are shown in Figure 4a observed during diffused reflectance spectroscopy analysis. The band gap values were calculated as 3.4 eV for Zn, 3.02 eV for Ag, and 2.95 eV for Neo-Ag/ZnO NC using the formula $E_{\rm g} = 1$, $240/\lambda$ abs. Diffused reflectance spectroscopy confirmed the nanoscale and

absorbance range of AgNPs [51–53] and ZnO NPs [54–56]. The absorbance shifts toward a longer wavelength confirmed the successful conjugation of the Neo drug to Ag/ZnO NC [57]. The agglomeration of NPs with the antibiotic, as well as the decrease in the energy gap between the excited state and the ground state, might be the reason for this red shift in UV [58]. The synthesized particles (Ag/ZnO NC) with the aforementioned band gap values can be employed as antimicrobial agents because of the easy penetration of nano-size particles into bacterial cells [59,60].

Figure 4b shows the FTIR spectra of Ag/ZnO NC, Neo-Ag/ ZnO NC, blank NEG (pure Carbopol NEG), Ag/ZnO NEG, and Neo-Ag/ZnO NEG. The capping of NPs by functional groups present in fungal extracts was confirmed by the presence of the amide group shown in FTIR spectra. Enzymes or proteins present in the cell-free culture filtrate can bind to NPs through their C₃H₇NO₂S cysteine or free amine group and provide stability to NPs, as reported earlier [61,62]. The fingerprint region of Ag/ZnO NC and Neo-Ag/ZnO was observed below 1,500 cm⁻¹. The peak at 1,336 cm⁻¹ might be due to the bending vibration of ZnO. The small absorption signal at 1,600 cm⁻¹ was assigned to the secondary amide (-NHR) in Ag/ZnO NC. The FTIR spectrum of Ag/ZnO NC displayed a weak intensity peak due to the incorporation of Ag⁺ with Zn²⁺. When Neo was conjugated with Ag/ZnO NC, the bending vibrational bands shifted to a lower wave number, at 1,033 cm⁻¹, and an extra peak at 3,000 cm⁻¹ confirmed the conjugation of Neo with Ag/ZnO NC.

The FTIR spectrum of blank NEG (unloaded Carbopol nanocarrier) showed a strong, broad O–H stretching vibration at 3,307 cm⁻¹, and this indicated the presence of a carboxylic acid group. The adsorption band at 2,884 cm⁻¹ could be attributed to the weak U-shaped aliphatic C–H stretching. The spectral region at 1,639 cm⁻¹ showed medium C=C stretching and weak C–O–C stretching at 1,350 and

10 — Zukhra Abbasi et al. DE GRUYTER

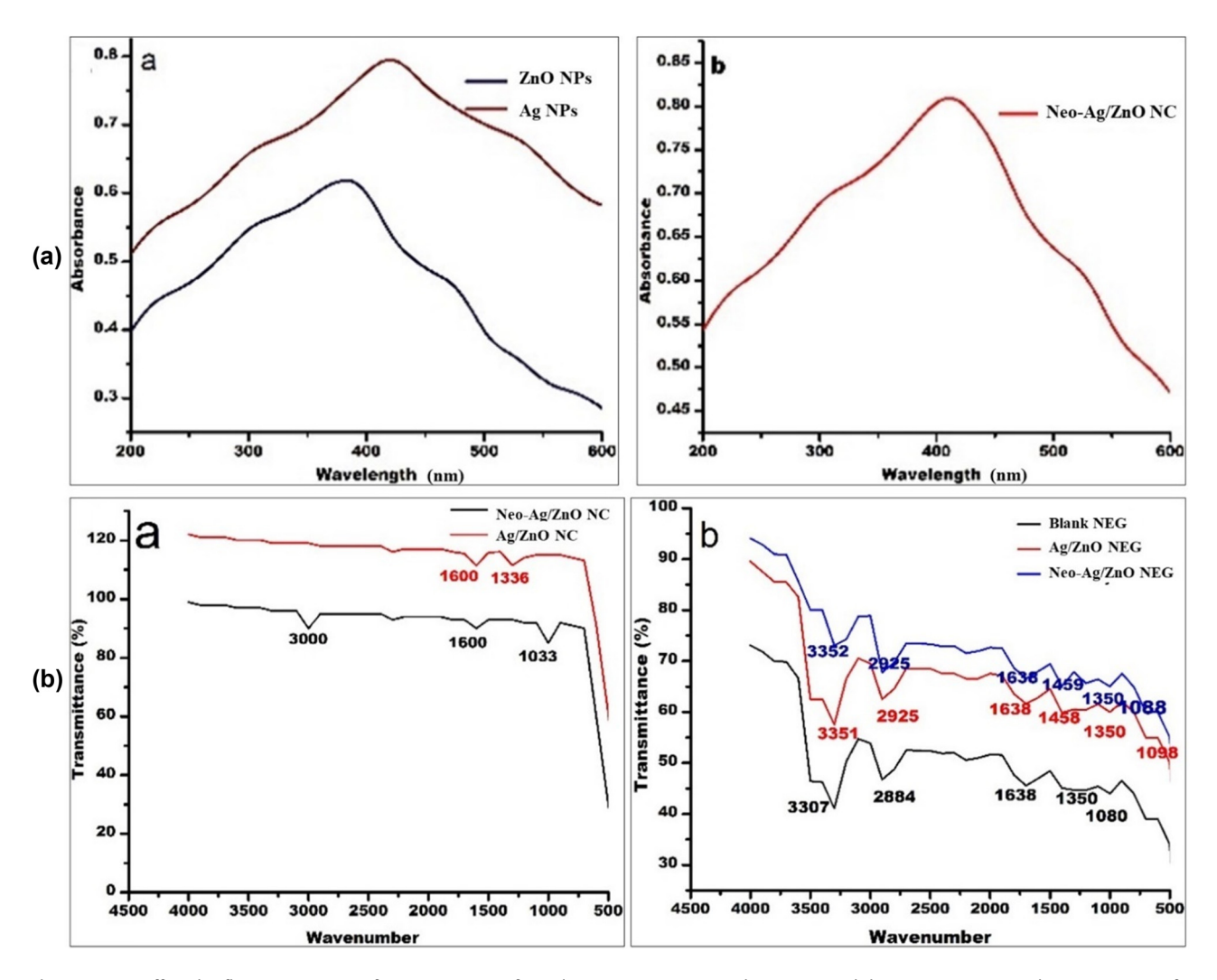


Figure 4: (a) Diffused reflectance spectra of mycogenic nanoformulations: ((a) Ag NPs and ZnO NPs and (b) Neo-Ag/ZnO NC). (b) FTIR spectra of mycogenic nanoformulations: ((a) Ag/ZnO NC and Neo-Ag/ZnO NC and (b) blank NEG, Ag/ZnO NEG and Neo-Ag/ZnO NEG).

1,080 cm⁻¹ owing to the presence of alkene and alkane groups in the Carbopol NEG. The FTIR spectrum of the Carbopol NEG (Blank NEG) is characterized by the presence of carboxylic acid, alkene, and alkane groups [24,63]. An additional peak is observed at 1,458 cm⁻¹ for Ag/ZnO NEG and at 1,459 cm⁻¹ for Neo-Ag/ZnO NEG. The presence of an additional peak and a band shift toward a longer wavelength after decoration with Ag/ZnO NC and Neo-Ag/ZnO NC indicated some physical interactions between the nanomaterial, the drug, and the Carbopol NEG, but this interaction did not affect the permeation of the nanomaterial, as indicated by the *in vitro* release study. Our data agree with a recent study that showed EU interaction with Carbopol NEG [24].

XRD analysis revealed sharp diffraction peaks, which indicates the crystallinity nature of the Neo-Ag/ZnO NC. A similar diffraction pattern was observed in a recent study

[10]. In accordance with JCPDS files (010891397 for ZnO. 030652871 for Ag), the XRD patterns of Ag/ZnO NC and Neo-Ag/ZnO NC showed lattice plane indices of 100, 002, 101, 111, 200, 102, 110, 103, 220, 112, and 201 related to the 2θ values 31.65, 35.0, 36.1, 38.0, 47.55, 56.55, 62.6, 67.3, 68.1, 69.7, and 78.1, respectively. Neo-Ag/ZnO NC showed similar peaks with a slight reduction in the peak intensity at planes 111 and 200 compared to that of Ag/ZnO NC; this revealed the amorphous nature of the Neo drug and the maintenance of the original NC structure (Figure 5a). Nevertheless, the dominant peaks associated with Ag/ZnO NC are of significantly higher magnitude, which may mask the presence of neomycin in the XRD pattern. This phenomenon underscores the challenge of detecting minor components in samples dominated by more abundant phases. Similar results were found in a study by El-Banna et al. [64], where they observed the absence of neomycin peak in the XRD

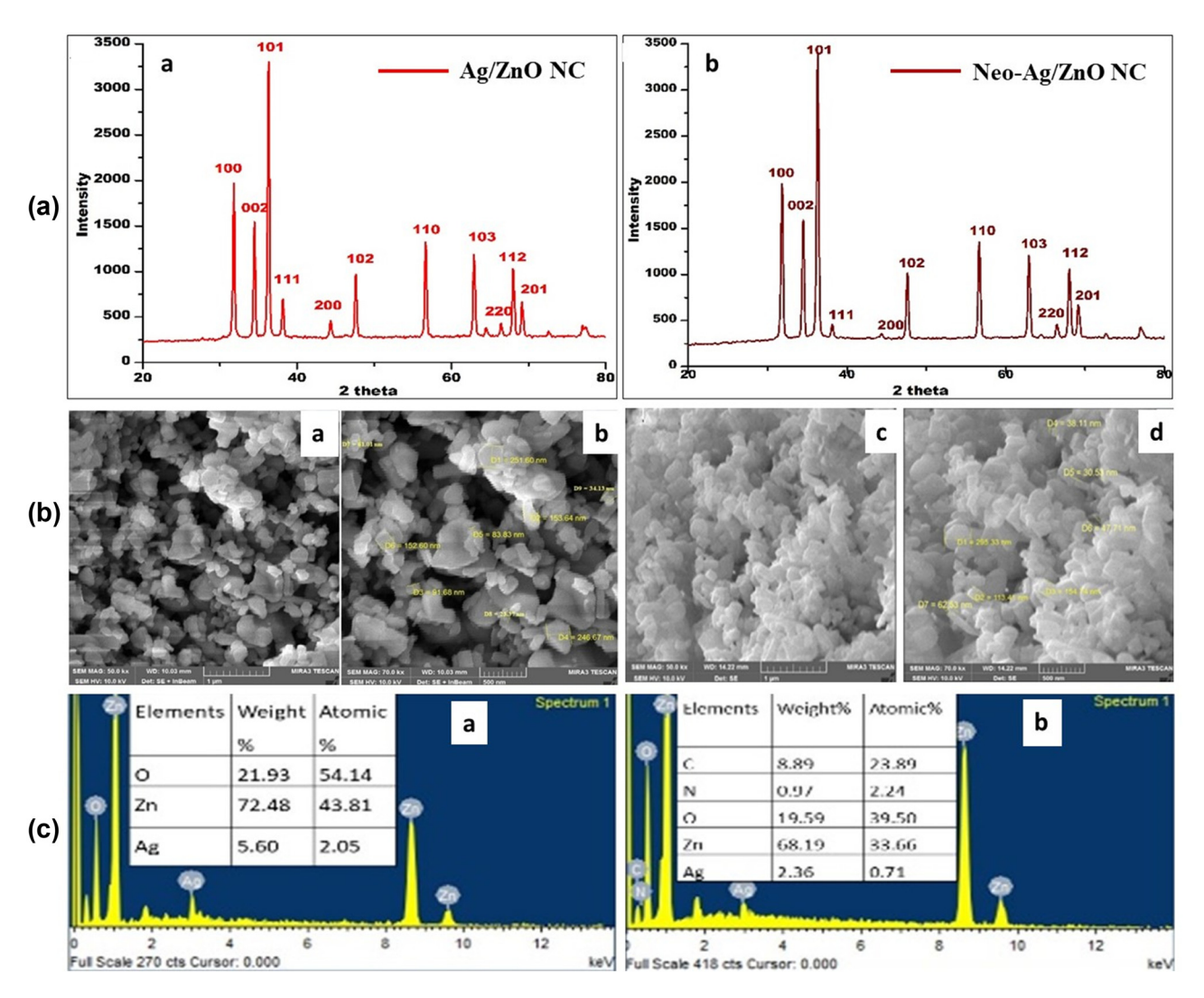


Figure 5: (a) XRD spectra of mycogenic nanoformulations: ((a) Ag/ZnO NC) and (b) Neo-Ag/ZnO NC)). (b) FESEM micrographs: ((a) Ag/ZnO NC at 1 μm, (b) Ag/ZnO NC at 500 nm), (c) Neo-Ag/ZnO NC at 1 μm, and (d) Neo-Ag/ZnO NC at 500 nm. (c) EDX spectra: ((a) Ag/ZnO NC) and (b) Neo-Ag/ZnO NC).

spectra of neomycin-silver nanocomposite gel. The average crystalline size of pure NC (Ag/ZnO NC) was 38 nm. It was 40 nm for the drug-conjugated NC (Neo-Ag/ZnO NC) calculated from the very sharp peak obtained with diffraction analysis corresponding to the plane (101) by applying the Debye–Scherrer formula. The size calculated by the Debye–Scherrer formula was quite similar to the size of the Ag/ZnO NC reported in previous studies [54,65]. Ag–ZnO NC with a size of less than 45 nm is less toxic to the epidermal cells of the skin, as reported by Das *et al.* and Majhi *et al.* [66,67]; hence, they can be used in topical wound care as antimicrobial agents.

Remarkably, the FESEM images (Figure 5b) depicted a diversity of shapes (rectangular, triangular, pentagonal, and sheet-like crystalline shapes) owing to the use of two different fungal strains and the significant release of many

different secondary metabolites that might act as reducing agents and ultimately impact NP properties. This observation is in line with the findings reported recently; indeed, two distinct morphologies for ZnO NPs with two different fungal strains were reported [68]. The average crystalline size of the pure NC (Ag/ZnO NC) and the drug-conjugated NC (Neo-Ag/ZnO NC) was 38 nm (range of 23-251 nm) and 40 nm (30-295 nm), respectively. The porosity increased with the increase in the PS, which is evident in the comparison between Neo-Ag/ZnO NC and pure Ag/ZnO NC. This increase in porosity was found to enhance the antimicrobial properties of Neo-Ag/ZnO NC against resistant strains, attributed to the higher surface area-to-volume ratio. This finding aligns with a study conducted by Bhosale et al., which demonstrated similar results [69]. They observed enhanced antibacterial and photocatalytic applications of

Table 1: Physical stability parameters of the mycosynthesized nanoformulations over 4 weeks

Time	Color change	Homogeneity	Phase separation	Consistency	Odor
Fresh	-ve	++++	-ve	++++	-ve
12 h	-ve	++++	-ve	++++	-ve
24 h	-ve	++++	-ve	++++	-ve
7 days	-ve	++++	-ve	++++	-ve
14 days	-ve	++++	-ve	++++	-ve
28 days	-ve	***	-ve	***	-ve

(++++) excellent; (+++) good; and (-ve) negative.

ZnONPs after doping with AgNPs, attributing this enhancement to an increase in porosity and surface area as PS increased [69]. Additionally, EDX spectra revealed the purity of the synthesized NPs as no extra peak was observed (Figure 5c). These data indicated the successful conjugation and absorption of the Neo drug in the NC. The Neo-Ag/ZnO NEG with an average PS of 215 nm and a polydispersity index (PDI) of 0.019 suggests both uniform PS distribution and homogeneous dispersion of the active pharmaceutical agent. Figure S9 shows a PS of 215 nm, within the range favorable for topical applications, facilitating enhanced drug penetration and release. Additionally, the low PDI value indicates consistent PS distribution, further supporting the formulation's suitability for efficient drug delivery in topical applications [38]

3.4 Organoleptic and stability features of the myconanoformulations

All the mycosynthesized nanoformulations (blank-NEG, Ag/ZnO NEG, and Neo-Ag/ZnO NEG) were inspected visually for organoleptic and stability features (Table 1). They were time-independent and similar in color compared to that of the freshly prepared Blank-NEG at different times: the color was creamy white for the Blank-NEG, light brownish for Ag/ZnO NEG, and greyish for Neo-Ag/ZnO NEG. The homogeneity and consistency were observed to be excellent; no differences in odor were observed, and no phase

separation (sedimentation) was seen upon centrifugation for the period of 28 days. Therefore, all the synthesized formulations were considered stable.

Statistically significant differences (p < 0.05) were observed in the pH values of fresh Ag/ZnO NEG (F2) and Neo-Ag/ZnO NEG (F3) in comparison with the fresh Blank-NEG (F1) after 12 h, as analyzed by one-way RM ANOVA (Table 2); this was due to the addition of triethanolamine. Also, F2 and F3 were slightly acidic (p > 0.05) compared to F1, and this may be due to the acidic nature of the nanomaterials added to F2 and F3. No other significant changes (p > 0.05) in pH from 12 h to day 28 were found in F1, F2, or F3, which denotes an overall pH stability. Overall, the pH values recorded were within the skin pH range of 5–6 and, thus, suitable for topical application [36]. All the values are expressed as mean \pm SEM.

Also, the viscosity determination is a fundamental step in evaluating emulgel formulations because it determines the permeability and bioavailability of bioactive molecules in topical DDS [36]. The unpaired t-test showed significant changes (p < 0.05) in the F1, F2, and F3 viscosities at low (6 rpm) and high (12 rpm) shear rates over the period of 28 days following non-Newtonian fluid (viscosity change with applied stress). F1 was significantly more viscous than F2 and F3 on different days (Table 3) since it was slightly acidic. The calculated spreadability value was $9.8 \pm 1.20 \, \text{s}$ for F1, while it was $10 \pm 1.25 \, \text{s}$ for F2 and $12.25 \pm 1.21 \, \text{s}$ for F3. The spreadability of F1 was lower compared to that of F2 and F3 due to its higher viscosity; conversely, the spreadability of F3 was higher compared to that of F1 and F2 due

Table 2: pH values of the mycosynthesized nanoformulations over 4 weeks

Formulations	рН						
	Fresh	12 h	24 h	7 days	14 days	28 days	
F1 (standard)	5.37 ± 0.0046	5.51 ± 0.0045	5.52 ± 0.005	5.53 ± 0.0046	5.53 ± 0.0051	5.53 ± 0.0046	
F2 (control)	5.35 ± 0.0045	5.49 ± 0.0051	5.50 ± 0.005	5.51 ± 0.005	5.51 ± 0.0046	5.51 ± 0.005	
F3 (test)	5.33 ± 0.005	5.47 ± 0.0046	5.46 ± 0.0051	5.47 ± 0.0051	5.47 ± 0.005	5.47 ± 0.0046	

Table 3: Viscosities (cP) of the mycosynthesized nanoformulations over 4 weeks

Shear rates (rpm)	Viscosity (in cP)							
	Fresh	12 h	24 h	7 days	14 days	28 days		
	F1 (Blank-NEG)							
6	5,598 ± 0.5	5,595 ± 0.454	5,593 ± 0.51	5,591 ± 0.51	5,590 ± 0.045	5,590 ± 0.51		
12	5,587 ± 0.046	5,583 ± 0.51	5,582 ± 0.046	5,581 ± 0.045	5,581 ± 0.51	5,580 ± 0.046		
	F2 (Ag/ZnO NEG)						
6	5,487 ± 0.51	5,487 ± 0.454	5,486 ± 0.045	5,485 ± 0.046	5,484 ± 0.454	5,483 ± 0.046		
12	5,473 ± 0.046	5,471 ± 0.51	5,471 ± 0.51	5,470 ± 0.046	5,470 ± 0.51	5,469 ± 0.5		
	F3 (Neo-Ag/ZnO NEG)							
6	5,410 ± 0.045	5,409 ± 0.046	5,409 ± 0.51	5,407 ± 0.046	5,407 ± 0.51	5,406 ± 0.5		
12	5,396 ± 0.51	5,396 ± 0.5	5,395 ± 0.046	5,393 ± 0.045	5,391 ± 0.451	5,390 ± 0.51		

to its lower viscosity. Herein, the rheological study showed that the synthesized nanoformulations followed a pseudoplastic behavior based on a recent study [70]. A decrease in viscosity at a high shear rate results in easier spreadability and improved pharmacodynamics after topical applications [71]. Viscosity of F1 > F2 > F3 (p < 0.05). Viscosity in F1 or F2 or F3 was overall stable (p > 0.05), as analyzed by unpaired t-test. All values are expressed as mean \pm SEM.

3.5 In vitro drug release behavior, drug content, hemocompatibility, and antimicrobial activity of Neo-Ag/ **ZnO NEG**

The most efficient nanoformulation, Neo-Ag/ZnO NEG (#F3), was assessed for its in vitro release and drug content. The in vitro study of Neo, ZnO, and Ag ions released from Neo-Ag/ ZnO NEG showed a slow and sustained release for 12 h. The cumulative release (Neo, ZnO, Ag) increased to 81% after 12 h (Figure S5). The in vitro release study showed a good pharmacokinetic profile of the mycosynthesized NEG; this was due to the optimum viscosity of 1% Carbopol 940 [72] and PEG, used as the permeation enhancer [73]. The release of a drug from an emulsion is controlled by the interaction of a drug with the emulsion's surfactant and co-surfactant; formulations with sustained release for a long time are preferred for topical delivery [36]. Any pharmaceutical dosage form must have an even distribution of pharmaceuticals to achieve a good interaction within the body, and this can be determined by finding the percentage of drug content. The drug content in Neo-Ag/ZnO NEG (F3) was as high as 98.70% obtained by RP-HPLC (Figure S6). The drug content in the F3 was found to be within the standard limit, and a relatively

good LC of the Carbopol emulgel with minimum drug loss during formulation was observed [36].

Besides, Neo-Ag/ZnO NEG (test, F3) exhibited no cytotoxicity against human erythrocytes (red blood cells - RBC) since no halo was observed (Figure S7). This was also the case for Neo (standard). A negligible (p > 0.05) RBC lysis zone (1 mm) was observed with 1× PBS (negative control). F3 was negligible (1 mm) compared to that of Triton-X 100 (positive control), which was 23 mm (p < 0.0001). The antimicrobial effects of the synthesized nanoformulations (i.e., Ag/ZnO NC, Neo-Ag/ZnO NC, blank NEG, Ag/ZnO NEG, and Neo-Ag/ ZnO NEG) against most of the prevalent MDR wound pathogens, such as P. aeruginosa, S. aureus, and C. albicans, were assessed by DDM (Figure 6a and Table 4) as well as by MIC (Figure 6b) and biofilm inhibition assay (Figure 6c). From DDM, B-NEG (Blank NEG) did not exhibit zones against selected strains. Prominent inhibition zones were observed for Ag/ZnO NC and the Neo-Ag/ZnO NEG, whereas Neo-Ag/ ZnO NEG showed the greatest antimicrobial potential against S. aureus, with an inhibition zone of 46 mm compared with other tested strains (p < 0.05) and compared to that of other tested nanoformulations (p < 0.05). The relative efficiency could be ordered as follows: Neo-Ag/ZnO NEG > Neo-Ag/ZnO NC > Ag/ZnO NEG > Ag/ZnO NC ≫ Neo (pure and validated antibiotic – see datasheet suppl. mat. file) >>> B-NEG when tested against P. aeruginosa, S. aureus, and C. albicans (Figure 6a and Table 4). F3 manifested superior antimicrobial properties compared to that of the Neo ointment (used as control) and the other mycosynthesized nanoformulations against selected microbial strains; this is most likely due to the successful incorporation and release of Neo, Ag⁺, and Zn²⁺ from NEG and its small (nano) size [36]. Such a nanoformulation could easily interact with the cell wall surface of microorganisms, resulting in DNA disruption, enzyme inactivation, and inhibition of protein synthesis by ROS

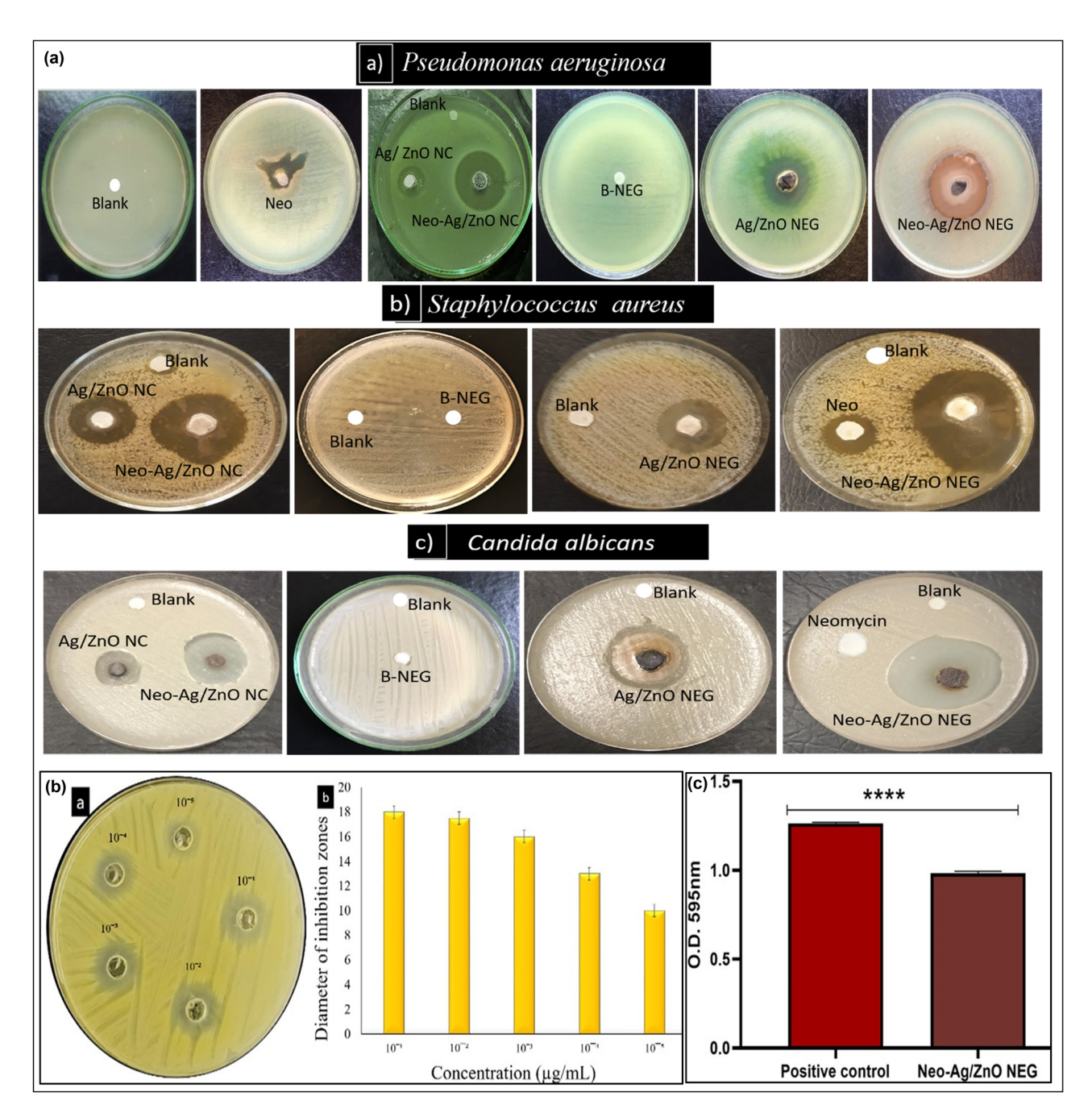


Figure 6: (a) Antimicrobial activity of samples against ((a) *P. aeruginosa*, (b) *S. aureus*, and (c) *C. albicans*). (b) MIC of Neo-Ag/ZnO NEG against MRSA: ((a) agar well diffusion plate and (b) graphical representation). (c) Antibiofilm activity of Neo-Ag/ZnO NEG against MRSA. Positive control: untreated microorganisms. Neo: neomycin; NC: ananocomposite; B-NEG: Blank NEG; NEG: nanoemulgel; Ag/ZnO: silver/zinc oxide.

formation [42]. These findings are in accordance with a recent study that used NEG for the topical delivery of Neo and reported an increase in the efficacy of Neo in terms of antibacterial activity after incorporating it into a tea tree oil-based nanoemulsion [74]. The MIC of Neo-Ag/ZnO NEG was $0.002\,\mu\text{g/mL}$ against MRSA, indicating that this test formulation (*F*3) was active at low concentrations (Figure 6b). The percentage of MRSA biofilm inhibition by Neo-Ag/ZnO NEG was 22%

(Figure 6c and Figure S8). Significant differences (p < 0.0001) were observed in the antibiofilm potential between the positive control (*i.e.*, untreated MRSA cells) and in Neo-Ag/ZnO NEG-treated MRSA cells. The small size and broad-spectrum activity of Neo, Ag, and ZnO led to an excellent biofilm inhibition potential against MRSA at MIC. Biocompatibility studies against human erythrocytes showed that Neo-Ag/ZnO NEG was safe for *in vivo* application in an animal model following the 3R

Table 4: Antimicrobial activity of mycosynthesized nanoformulations

Strains tested	Diameter of growth inhibition zones (mm)								
	Formulation codes								
	Blank	Neo	Ag/ZnO NC	Neo-Ag/ZnO NC	B-NEG	Ag/ZnONEG	Neo-Ag/ZnO NEG		
P. aeruginosa	_	9 ± 0.5	15 ± 0.46	27 ± 0.46	_	24 ± 0.45	31 ± 0.51		
S. aureus	_	13 ± 0.54	28 ± 0.51	39 ± 0.54	_	30 ± 0.46	46 ± 0.45		
C. albicans	_	_	20 ± 0.51	25 ± 0.46	_	32 ± 0.51	42 ± 0.45		

Neo: neomycin; NC: nanocomposite; B-NEG: Blank NEG; NEG: nanoemulgel. All values are expressed as the mean ± SEM.

principles (*i.e.*, Replacement, Reduction, and Refinement) in animal research.

3.6 In vivo wound healing

Neo-Ag/ZnO NEG had excellent wound-healing activity in mice when compared with the control (untreated wound).

Indeed, the WTC achieved by Neo-Ag/ZnO NEG was found to be markedly higher (100%) compared to that of the control (55%) on day 12. Because of skin contraction and fast skin re-epithelialization, WTC was observed from day 4 onward with a concentration as low as 0.01% of 100 mg Neo-Ag/ZnO NEG. Treated mice showed a significant (p=0.0001) increase in wound contraction either on day 4, day 8, or day 12 in comparison to the control. No itching,

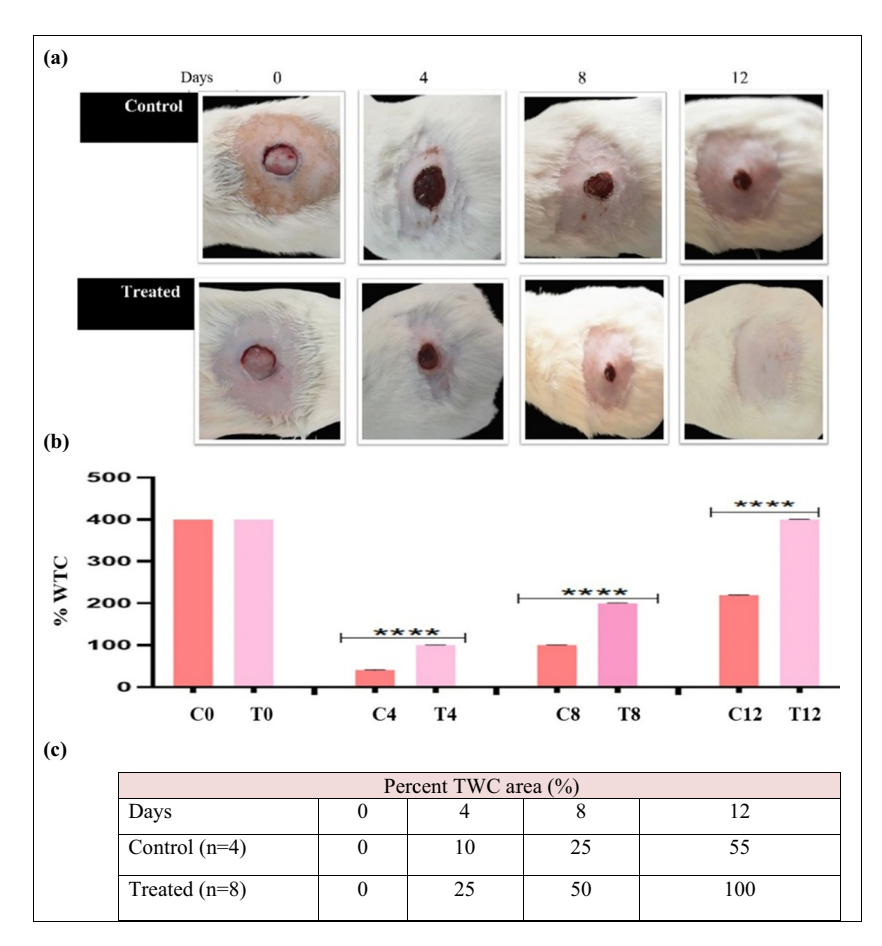


Figure 7: *In vivo* (in mice) wound-healing potential of Neo-Ag/ZnO NEG over a period of 12 days. (a) Pictures were taken at 4-day interval after treatment with Neo-Ag/ZnO NEG. (b) Graphical representation of the Neo-Ag/ZnO NEG effect on wound area (mm²) at indicated days. Data are presented as the mean \pm SEM. N = 12 (****p = 0.0001). (c) Tabulated data. WTC: wound total closure.

irritation, or inflammation was observed. Pictures, graphical representation, and tabulated data representing wound closure on various days are summarized in Figure 7a–c, respectively.

3.7 Hypothetical wound infection and healing mechanism

When the skin's integrity is compromised, whether through surgery or physical trauma, microbes from the skin surface invade the wound site, initiating colonization and releasing toxins, eventually forming a biofilm. This impedes immune cells like macrophages and neutrophils from effectively eliminating the microbes, leading to persistent inflammation and disrupting collagen synthesis [75] as shown in Figure 8a. Oral antibiotics are not recommended as microbes build tolerance against antibiotics [76]. Hence, our synthesized Neo-Ag/ZnO NEG offers a solution by gradually releasing nano-antibiotics from the Carbopol NEG at the wound site as shown Figure 8b, effectively eradicating biofilms and killing microbes due to its broad-spectrum antimicrobial properties by ROS production. Moreover, the NEG prevents microbial entry, mitigates infection, promotes collagen deposition and maintains

optimal moisture levels for wound contraction. This facilitates immune cell migration to the wound site with neoangiogenesis and skin cell formation, promoting early wound healing [36]. In a recent research, Majhi et al. stated that Ag/ZnO NPs stimulate the production of antimicrobial peptides and enhance the migration and antibacterial abilities of keratinocytes, which can potentially aid in wound healing and combating bacterial infection [67]. In comparison to prior studies, our research findings align with previous evidence indicating that Ag/ZnO NPs stimulate the production of antimicrobial peptides and enhance the migratory and antibacterial capabilities of skin cells (keratinocytes) against S. aureus. This consistency reinforces the potential therapeutic utility of Ag/ZnO NPs in promoting wound healing and combating bacterial infections. However, it is noteworthy that our study contributes novel insights by specifically highlighting the effectiveness of Carbopol NEG.

4 Conclusions

We report a novel and cost-effective fungal consortiumbased synthesis of an Ag/ZnO NEG, which could be used as an effective topical antibiotic drug nanocarrier to

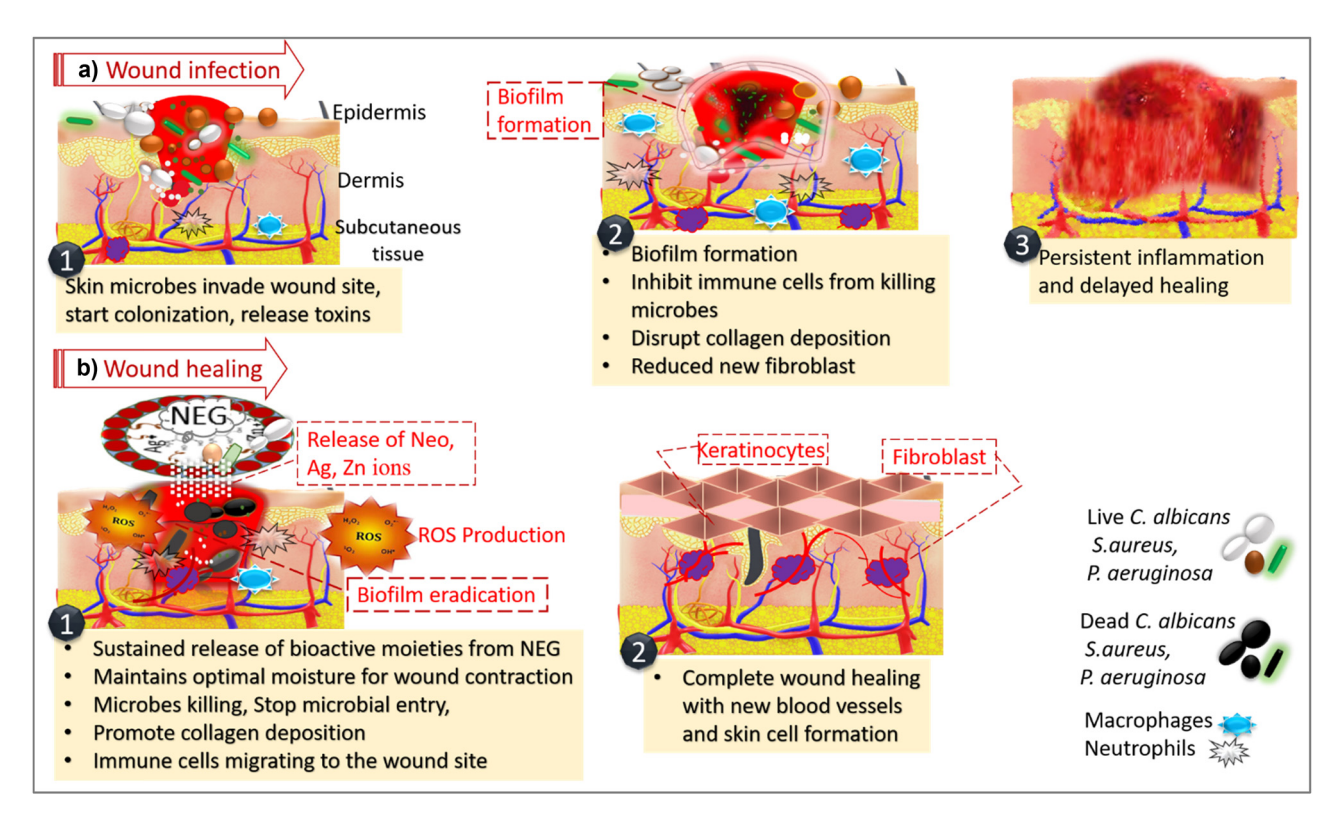


Figure 8: Illustration of putative skin wound infection mechanism by microbes (a). Neo-Aq/ZnO NEG-induced wound healing mechanisms (b).

overcome resistant skin infections and boost the skin healing process. To the best of our knowledge, this is a pioneered study. We have shown that it is possible to produce a relatively high yield of Ag/ZnO NC and stabilize it with the polymer matrix Carbopol after encapsulation with Neo. FTIR studies confirmed the incorporation of the drug and NPs (Ag and ZnO) into the prepared NEG. The release profile, pH, viscosity, spreadability, and hemocompatibility tests revealed that the Neo-Ag/ZnO NEG was suitable for topical delivery. Remarkably, Neo-Ag/ZnO NEG showed broader-spectrum activity against MDR wound pathogens in vitro compared to that of Neo and Neo-Ag/ZnO NC. Neo-Ag/ZnO NEG showed the highest activity (46 mm) against S. aureus and was prominent against MRSA. Importantly, Neo-Ag/ZnO NEG elicited a huge and safe wound-healing potential in mice, most likely due to its small size, stability, and sustained release of the NPs. We propose that the current Neo-Ag/ZnO NEG formulation is a promising topical NDDS for infected wound management due to its sustained and targeted release of bioactive nanomaterials.

5 Future directions

In future research, exploring the potential of the green fabricated nanoparticle-embedded GEL (NEG) could involve investigating its antimicrobial, anti-inflammatory, and antioxidant properties through in vivo studies. Additionally, conducting further cytotoxicity assays on animal models and cell lines is recommended to ensure long-term safety, biocompatibility, and potential adverse effects of the NEG (NDDS), thereby paving the way for subsequent clinical trials. Furthermore, mechanistic studies elucidating its mode of action in facilitating wound healing would offer valuable insights for clinical translation. Pursuing these avenues may offer significant advancements in wound management and infection control. Concurrently, investigating the compatibility of this NDDS with other antimicrobial agents for combination therapy could offer enhanced treatment strategies against a broader spectrum of microbial challenges and mitigate AMR.

Acknowledgments: The authors are thankful to the Deanship of Research and Graduate Studies, King Khalid University, Abha, Saudi Arabia, for financially supporting this work through the Large Research Group Project under Grant no. R.G.P.2/42/45.

Funding information: This research was supported by International Islamic University, Pakistan, under grant number 2018/0046-IIU.

Author contributions: Conceptualization: Z.A., B.U.; writing - original draft preparation: Z.A., F.M.; methodology, software, validation, formal analysis, investigation, data curation: Z.A., B.U., B.A.K., F.F.; S.M.A., F.M.; visualization, supervision, and project administration: B.U.; resources and funding acquisition: B.U.; writing-review and editing, and submission: F.M. All authors have accepted responsibility for the entire content of this manuscript and approved its submission.

Conflict of interest: The authors state no conflict of interest.

Ethical approval: The study was conducted according to the guidelines of the Declaration of Helsinki and approved by the Institutional Review Board (or Ethics Committee) of the Department of Biological Sciences Ethics and Biosafety Committee of International Islamic University Islamabad, Pakistan (protocol code Reg #470-FBAS/MSBT/F-20, date of approval 12/27/21). The blood sample was provided by a healthy human with written informed consent and kept confidential throughout the experiment. All precautions have been undertaken to minimize the suffering of animals.

References

- Talebi Bezmin Abadi A, Rizvanov AA, Haertlé T, Blatt NL. World Health Organization report: current crisis of antibiotic resistance. BioNanoSci. 2019 Dec;9(4):778-88. doi: 10.1007/s12668-019-
- [2] Boero E, Mnich ME, Manetti AG, Soldaini E, Grimaldi L, Bagnoli F. Human three-dimensional models for studying skin pathogens. Three dimensional human organotypic models for biomedical research. Curr Top Microbiol Immunol. 2021;430(3-27):3-27. doi: 10.1007/82_2020_219.
- FrykbergRobert G, Banks J. Challenges in the treatment of chronic [3] wounds. Adv Wound Care. 2015 Aug;4:560-82 (New Rochelle). doi: 10.1089/wound.2015.0635.
- Nešporová K, Pavlík V, Šafránková B, Vágnerová H, Odráška P, [4] Žídek O, et al. Effects of wound dressings containing silver on skin and immune cells. Sci Rep. 2020 Sep;10(1):15216. doi: 10.1038/ s41598-020-72249-3.
- Giurazza R, Mazza MC, Andini R, Sansone P, Pace MC, Durante-[5] Mangoni E. Emerging treatment options for multi-drug-resistant bacterial infections. Life. 2021 Jun;11(6):519. doi: 10.3390/ life11060519.
- [6] Komal R, Uzair B, Sajjad S, Butt S, Kanwal A, Ahmed I, et al. Skirmishing MDR strain of Candida albicans by effective antifungal CeO2 nanostructures using Aspergillus terreus and Talaromyces purpurogenus. Mater Res Express. 2020 May;7(5):055004. doi: 10. 1088/2053-1591/ab8ba2.
- Ahmed EF, Rasmi AH, Darwish AM, Gad GF. Prevalence and resistance profile of bacteria isolated from wound infections among a group of patients in upper Egypt: a descriptive cross-sectional

- study. BMC Res Notes. 2023 Jun;16(1):106. doi: 10.1186/s13104-023-06379-v.
- [8] Pammi SV, Padavala VS, Karumuri TS, Kommavari CS, Shaik M, Kolapalli VR, et al. Wound healing synergy in Wistar albino rats via green synthesized nanoparticles and topical antibiotic neomycin. OpenNano. 2023 May;11:100135. doi: 10.1016/j.onano.2023.100135.
- [9] Loo YY, Rukayadi Y, Nor-Khaizura MA, Kuan CH, Chieng BW, Nishibuchi M, et al. *In vitro* antimicrobial activity of green synthesized silver nanoparticles against selected gram-negative foodborne pathogens. Front Microbiol. 2018 Jul;9:1555. doi: 10.3389/ fmicb 2018.01555.
- [10] González Cuadra J, Vicedo Jover B, Scalschi LM, Guc M, Izquierdo-Roca V, Porcar García S, et al. Zno/Ag nanocomposites with enhanced antimicrobial activity. Appl Sci. 2022 May;12:5023. SSRN 4036165. doi: 10.3390/app12105023.
- [11] Matai I, Sachdev A, Dubey P, Kumar SU, Bhushan B, Gopinath P. Antibacterial activity and mechanism of Ag–ZnO nanocomposite on S. aureus and GFP-expressing antibiotic resistant E. coli. Colloids Surf B Biointerfaces. 2014 Mar;115:359–67. doi: 10.1016/j.colsurfb. 2013.12.005.
- [12] Jain D, Shivani, Bhojiya AA, Singh H, Daima HK, Singh M, et al. Microbial fabrication of zinc oxide nanoparticles and evaluation of their antimicrobial and photocatalytic properties. Front Chem. 2020 Sep;8:778. doi: 10.3389/fchem.2020.00778.
- [13] Vijayaram S, Razafindralambo H, Sun YZ, Vasantharaj S, Ghafarifarsani H, Hoseinifar SH, et al. Applications of green synthesized metal nanoparticles – a review. Biol Trace Elem Res. 2024 Jan;202(1):360–86. doi: 10.1007/s12011-023-03645-9.
- [14] Wang D, Xue B, Wang L, Zhang Y, Liu L, Zhou Y. Fungus-mediated green synthesis of nano-silver using *Aspergillus sydowii* and its antifungal/antiproliferative activities. Sci Rep. 2021 May;11(1):10356. doi: 10.1038/s41598-021-89854-5.
- [15] Nassar AR, Atta HM, Abdel-Rahman MA, El Naghy WS, Fouda A. Myco-synthesized copper oxide nanoparticles using harnessing metabolites of endophytic fungal strain Aspergillus terreus: an insight into antibacterial, anti-Candida, biocompatibility, anticancer, and antioxidant activities. BMC Complement Med Ther. 2023 Jul;23(1):261. doi: 10.1186/s12906-023-04056-y.
- [16] Kalyani RL, Kumar KS, Swamy PV, Sekhar KC, Manish S, Murthy KR, et al. Synergetic potential of green synthesized nano-antibiotic combinational therapy for wound healing. Res Sq. 2021. doi: 10. 21203/rs.3.rs-1204154/v1.
- [17] Yoon DJ, Nguyen C, Bagood MD, Fregoso DR, Yang HY, Lopez AI, et al. Topical fluoxetine as a potential nonantibiotic adjunctive therapy for infected wounds. J Invest Dermatol. 2021 Jun;141(6):1608–12.e3. doi: 10.1016/j.jid.2020.11.016.
- [18] Veirup N, Kyriakopoulos C. Neomycin. [Updated 2022 May 8]. In: StatPearls [Internet]. Treasure Island (FL): StatPearls Publishing; 2022 Jan. https://www.ncbi.nlm.nih.gov/books/NBK560603/.
- [19] Benson HA, Grice JE, Mohammed Y, Namjoshi S, Roberts MS. Topical and transdermal drug delivery: from simple potions to smart technologies. Curr Drug Deliv. 2019 Jun;16(5):444–60. doi: 10. 2174/1567201816666190201143457.
- [20] Aithal GC, Narayan R, Nayak UY. Nanoemulgel: A promising phase in drug delivery. Curr Pharm Des. 2020 Jan;26(2):279–91. doi: 10. 2174/138161282666619122610024.
- [21] Gaber DA, Alsubaiyel AM, Alabdulrahim AK, Alharbi HZ, Aldubaikhy RM, Alharbi RS, et al. Nanoemulsion based gel for topical delivery of an anti-inflammatory drug: *In vitro* and *in vivo*

- evaluation. Drug Des Devel Ther. 2023 Dec;17:1435–51. doi: 10.2147/DDDT.S407475.
- [22] Donthi MR, Munnangi SR, Krishna KV, Saha RN, Singhvi G, Dubey SK. Nanoemulgel: a novel nano carrier as a tool for topical drug delivery. Pharmaceutics. 2023 Jan;15(1):164. doi: 10.3390/ pharmaceutics15010164.
- [23] Medina-Cruz D, Saleh B, Vernet-Crua A, Ajo A, Roy AK, Webster TJ. Drug-delivery nanocarriers for skin wound-healing applications. In: Wound healing, tissue repair, and regeneration in diabetes. Elsevier; 2020 Jan. p. 439–488. Academic Press. doi: 10.1016/b978-0-12-816413-6.00022-8.
- [24] Rehman A, Iqbal M, Khan BA, Khan MK, Huwaimel B, Alshehri S, et al. Fabrication, in vitro, and in vivo assessment of eucalyptolloaded nanoemulgel as a novel paradigm for wound healing. Pharmaceutics. 2022 Sep;14(9):1971. doi: 10.3390/pharmaceutics14091971.
- [25] Bibi S, Mir S, Rehman W, Menaa F, Gul A, Alaryani FS, et al. Synthesis and in vitro/ex vivo characterizations of ceftriaxone-loaded sodium alginate/poly (vinyl alcohol) clay reinforced nanocomposites: possible applications in wound healing. Materials. 2022 May;15(11):3885. doi: 10.3390/ma15113885.
- [26] Razzaq A, Khan ZU, Saeed A, Shah KA, Khan NU, Menaa B, et al. Development of cephradine-loaded gelatin/polyvinyl alcohol electrospun nanofibers for effective diabetic wound healing: in vitro and in vivo assessments. Pharmaceutics. 2021 Mar;13(3):349. doi: 10.3390/pharmaceutics13030349.
- [27] Khan BA, Ullah S, Khan MK, Uzair B, Menaa F, Braga VA. Fabrication, physical characterizations, and in vitro, in vivo evaluation of ginger extract-loaded gelatin/poly (vinyl alcohol) hydrogel films against burn wound healing in animal model. AAPS PharmSciTech. 2020 Nov;21(8):323. doi: 10.1208/s12249-020-01866-y.
- [28] Akram MA, Khan BA, Khan MK, Alqahtani A, Alshahrani SM, Hosny KM. Fabrication and characterization of polymeric pharmaceutical emulgel co-loaded with eugenol and linalool for the treatment of trichophyton rubrum infections. Polymers. 2021 Nov;13(22):3904. doi: 10.3390/polym13223904.
- [29] Khalil AM, Hassan SE, Alsharif SM, Eid AM, Ewais EE, Azab E, et al. Isolation and characterization of fungal endophytes isolated from medicinal plant Ephedra pachyclada as plant growth-promoting. Biomol. 2021 Jan;11(2):140. doi: 10.3390/biom11020140.
- [30] Moubasher AH, Moustafa AF. A survey of Egyptian soil fungi with special reference to Aspergillus, Pénicillium and Penicillium-related genera. Trans Br Mycological Soc. 1970;54:35–44. doi: 10.1016/ S0007-1536(70)80121-8.
- [31] Woudenberg JH, Groenewald JZ, Binder M, Crous PW. Alternaria redefined. Stud mycology. 2013 Jun;75(1):171–212. doi: 10.3114/ sim0015.
- [32] Castro P, Parada R, Corrial C, Mendoza L, Cotoras M. Endophytic fungi isolated from *Baccharis linearis* and *Echinopsis chiloensis* with antifungal activity against *Botrytis cinerea*. J Fungi. 2022 Feb;8(2):197. doi: 10.3390/jof8020197.
- [33] Consolo VF, Torres-Nicolini A, Alvarez VA. Mycosinthetized Ag, CuO and ZnO nanoparticles from a promising *Trichoderma harzianum* strain and their antifungal potential against important phytopathogens. Sci Rep. 2020 Nov;10(1):20499. doi: 10.1038/s41598-020-77294-6.
- [34] Abid S, Uzair B, Niazi MB, Fasim F, Bano SA, Jamil N, et al. Bursting the virulence traits of MDR strain of *Candida albicans* using sodium alginate-based microspheres containing nystatin-loaded MgO/CuO

- nanocomposites. Int J Nanomed. 2021 Feb;16:1157–74. doi: 10.2147/ IJN.S282305.
- [35] Hosny KM, Naveen NR, Kurakula M, Sindi AM, Sabei FY, Fatease AA, et al. Design and development of neomycin sulfate gel loaded with solid lipid nanoparticles for buccal mucosal wound healing. Gels. 2022 Jun;8(6):385. doi: 10.3390/gels8060385.
- [36] Khan BA, Ali A, Hosny KM, Halwani AA, Almehmady AM, Iqbal M, et al. Carbopol emulgel loaded with ebastine for urticaria: Development, characterization, in vitro and in vivo evaluation. Drug Deliv. 2022 Dec;29(1):52–61. doi: 10.1080/10717544.2021.2015483.
- [37] Zafar N, Uzair B, Niazi MB, Menaa F, Samin G, Khan BA, et al. Green synthesis of ciprofloxacin-loaded cerium oxide/chitosan nanocarrier and its activity against MRSA-induced mastitis. J Pharm Sci. 2021 Oct:110(10):3471–83. doi: 10.1016/j.xphs.2021.06.017.
- [38] Khan BA, Ahmad N, Alqahtani A, Baloch R, Rehman AU, Khan MK. Formulation development of pharmaceutical nanoemulgel for transdermal delivery of feboxostat: Physical characterization and in vivo evaluation. Eur J Pharm Sci. 2024c Apr;195:106665. doi: 10.1016/ j.ejps.2023.106665.
- [39] Haq S, Rashid M, Menaa F, Shahzad N, Shahzad MI, Alfaifi SY, et al. Antibacterial and antioxidant screening applications of reduced-graphene oxide modified ternary SnO₂-NiO-CuO nanocomposites. Arab J Chem. 2023 Aug;16(8):104917. doi: 10.1016/J.ARABJC.2023. 104917.
- [40] Burki IK, Khan MK, Khan BA, Uzair B, Braga VA, Jamil QA. Formulation development, characterization, and evaluation of a novel dexibuprofen-capsaicin skin emulgel with improved in vivo anti-inflammatory and analgesic effects. AAPS PharmSciTech. 2020 Aug;21:1–4. doi: 10.1208/s12249-020-01760-7.
- [41] Uzair B, Ahmed N, Ahmad VU, Kousar F. A new antibacterial compound produced by an indigenous marine bacteria—fermentation, isolation, and biological activity. Nat Prod Res. 2006 Dec;20(14):1326–31. doi: 10.1080/14786410601102017.
- [42] Abbas S, Uzair B, Sajjad S, Leghari SA, Noor S, Niazi MB, et al. Dual-functional green facile CuO/MgO nanosheets composite as an efficient antimicrobial agent and photocatalyst. Arab J Sci Eng. 2022 May;47(5):5895–909. doi: 10.1007/s13369-021-05741-1.
- [43] Gonelimali FD, Lin J, Miao W, Xuan J, Charles F, Chen M, et al.

 Antimicrobial properties and mechanism of action of some plant extracts against food pathogens and spoilage microorganisms.

 Front Microbiol. 2018 Jul;9:1639. doi: 10.3389/fmicb.2018.01639.
- [44] Uzair B, Akhtar N, Sajjad S, Bano A, Fasim F, Zafar N, et al. Targeting microbial biofilms: by *Arctium lappa* I. synthesised biocompatible CeO2-NPs encapsulated in nano-chitosan. IET Nanobiotechnol. 2020 May;14(3):217–23. doi: 10.1049/iet-nbt.2019.0294.
- [45] Iqbal H, Razzaq A, Uzair B, Ul Ain N, Sajjad S, Althobaiti NA, et al. Breast cancer inhibition by biosynthesized titanium dioxide nanoparticles is comparable to free doxorubicin but appeared safer in BALB/c mice. Materials. 2021 Jun;14(12):3155. doi: 10.3390/ma14123155.
- [46] Chen L, Mirza R, Kwon Y, DiPietro LA, Koh TJ. The murine excisional wound model: Contraction revisited. Wound Repair Regen. 2015 Nov;23(6):874–7. doi: 10.1111/wrr.12338.
- [47] Sadiq T, Khalid SH, Khan IU, Mahmood H, Asghar S. Designing deferoxamine-loaded flaxseed gum and carrageenan-based controlled release biocomposite hydrogel films for wound healing. Gels. 2022 Oct;8(10):652. doi: 10.3390/gels8100652.
- [48] Macedo AS, Mendes F, Filipe P, Reis S, Fonte P. Nanocarrier-mediated topical insulin delivery for wound healing. Materials. 2021 Jul;14(15):4257. doi: 10.3390/ma14154257.

- [49] Yoo S, Nam DH, Singh TI, Leem G, Lee S. Effect of reducing agents on the synthesis of anisotropic gold nanoparticles. Nano Converg. 2022 Jan;9(1):5. doi: 10.1186/s40580-021-00296-1.
- [50] Saddik MS, Elsayed MM, El-Mokhtar MA, Sedky H, Abdel-Aleem JA, Abu-Dief AM, et al. Tailoring of novel Azithromycin-loaded zinc oxide nanoparticles for wound healing. Pharmaceutics. 2022 Jan;14(1):111. doi: 10.3390/pharmaceutics1401011.
- [51] Mohamed JM, Alqahtani A, Kumar TV, Fatease AA, Alqahtani T, Krishnaraju V, et al. Superfast synthesis of stabilized silver nanoparticles using aqueous Allium sativum (garlic) extract and isoniazid hydrazide conjugates: molecular docking and in vitro characterizations. Molecules. 2021 Dec;27(1):110. doi: 10.3390/ molecules27010110.
- [52] Arif W, Rana NF, Saleem I, Tanweer T, Khan MJ, Alshareef SA, et al. Antibacterial activity of dental composite with ciprofloxacin loaded silver nanoparticles. Molecules. 2022 Oct;27(21):7182. doi: 10.3390/ molecules27217182
- [53] Azhar S, Rana NF, Kashif AS, Tanweer T, Shafique I, Menaa F. DEAE-Dextran Coated AgNPs: A Highly Blendable Nanofiller Enhances Compressive Strength of Dental Resin Composites. Polymers. 2022 Aug;14(15):3143. doi: 10.3390/polym14153143.
- [54] Tanweer T, Rana NF, Saleem I, Shafique I, Alshahrani SM, Almukhlifi HA, et al. Dental composites with magnesium doped zinc oxide nanoparticles prevent secondary caries in the alloxaninduced diabetic model. Int J Mol Sci. 2022 Dec;23(24):15926. doi: 10.3390/ijms232415926.
- [55] Ahmed SS, Alqahtani AM, Alqahtani T, Alamri AH, Menaa F, Mani RK, et al. Green synthesis, characterizations of zinc oxide nanoparticles from aqueous leaf extract of *Tridax procumbens* Linn. and Assessment of their anti-hyperglycemic activity in streptozoticin-induced diabetic rats. Materials. 2022 Nov 18;15(22):8202. doi: 10.3390/ma15228202.
- [56] Raja A, Ashokkumar S, Marthandam RP, Jayachandiran J, Khatiwada CP, Kaviyarasu K, et al. Eco-friendly preparation of zinc oxide nanoparticles using Tabernaemontana divaricata and its photocatalytic and antimicrobial activity. J Photochem Photobiol B. 2018 Apr;181:53–8. doi: 10.1016/j.jphotobiol.2018.02.011.
- [57] Ansari SA, Cho MH. Highly visible light responsive, narrow band gap TiO₂ nanoparticles modified by elemental red phosphorus for photocatalysis and photoelectrochemical applications. Sci Rep. 2016a May;6(1):25405. doi: 10.1038/srep25405.
- [58] Perveen S, Safdar N, Chaudhry GE, Yasmin A. Antibacterial evaluation of silver nanoparticles synthesized from lychee peel: individual versus antibiotic conjugated effects. World J Microbiol Biotechnol. 2018 Aug;34(8):118. doi: 10.1007/s11274-018-2500-1.
- [59] Wang L, Hu C, Shao L. The antimicrobial activity of nanoparticles: present situation and prospects for the future. Int J Nanomed. 2017 Feb;12:1227–49. doi: 10.2147/IJN.S121956.
- [60] Ansari SA, Ansari SG, Foaud H, Cho MH. Facile and sustainable synthesis of carbon-doped ZnO nanostructures towards the superior visible light photocatalytic performance. N J Chem. 2017;41(17):9314–20. doi: 10.1039/C6NJ04070E.
- [61] Jaidev LR, Narasimha G. Fungal mediated biosynthesis of silver nanoparticles, characterization and antimicrobial activity. Colloids Surf B Biointerfaces. 2010 Dec;81(2):430–3. doi: 10.1016/j.colsurfb. 2010.07.033
- [62] Thapa R, Bhagat C, Shrestha P, Awal S, Dudhagara P. Enzymemediated formulation of stable elliptical silver nanoparticles tested against clinical pathogens and MDR bacteria and development of

- antimicrobial surgical thread. Ann Clin Microbiol Antimicrob. 2017 Dec;16(39):1. doi: 10.1186/s12941-017-0216-y.
- [63] Jana S, Manna S, Nayak AK, Sen KK, Basu SK. Carbopol gel containing chitosan-egg albumin nanoparticles for transdermal aceclofenac delivery. Colloids Surf B Biointerfaces. 2014 Feb;114:36–44. doi: 10.1016/j.colsurfb.2013.09.045.
- [64] El-Banna AH, Youssef FS, Youssef Elzorba H, Soliman AM, Mohamed GG, Ismail SH, et al. Evaluation of the wound healing effect of neomycin-silver nanocomposite gel in rats. Int J Immunopathol Pharmacol. 2022 Jul;36:03946320221113486. doi: 10.1177/03946320221113486.
- [65] Primo JD, Horsth DF, Correa JD, Das A, Bittencourt C, Umek P, et al. Synthesis and characterization of Ag/ZnO nanoparticles for bacteria disinfection in water. Nanomaterials. 2022 May;12(10):1764. doi: 10.3390/nano12101764.
- [66] Das B, Khan MI, Jayabalan R, Behera SK, Yun SI, Tripathy SK, et al. Understanding the antifungal mechanism of Ag@ ZnO core-shell nanocomposites against *Candida krusei*. Sci Rep. 2016 Nov;6(1):36403. doi: 10.1038/srep36403.
- [67] Majhi RK, Mohanty S, Khan MI, Mishra A, Brauner A. Ag@ ZnO nanoparticles induce antimicrobial peptides and promote migration and antibacterial activity of keratinocytes. ACS Infect Dis. 2021 Mar;7(8):2068–72. doi: 10.1021/acsinfecdis.0c00903.
- [68] Mohamed AA, Fouda A, Abdel-Rahman MA, Hassan SE, El-Gamal MS, Salem SS, et al. Fungal strain impacts the shape, bioactivity and multifunctional properties of green synthesized zinc oxide nanoparticles. Biocatal Agric Biotechnol. 2019 May;19:101103. doi: 10.1016/j.bcab.2019.101103.
- [69] Bhosale A, Kadam J, Gade T, Sonawane K, Garadkar K. Efficient photodegradation of methyl orange and bactericidal activity of Ag

- doped ZnO nanoparticles. J Indian Chem Soc. 2023 Feb;100(2):100920. doi: 10.1016/j.jics.2023.100920.
- [70] Kazim T, Tariq A, Usman M, Ayoob MF, Khan A. Chitosan hydrogel for topical delivery of ebastine loaded solid lipid nanoparticles for alleviation of allergic contact dermatitis. RSC Adv. 2021;11(59):37413–25. doi: 10.1039/D1RA06283B.
- [71] Md S, Alhakamy NA, Aldawsari HM, Kotta S, Ahmad J, Akhter S, et al. Improved analgesic and anti-inflammatory effect of diclofenac sodium by topical nanoemulgel: Formulation development – In vitro and in vivo studies. J Chem. 2020 Oct;2020:4071818. doi: 10. 1155/2020/4071818
- [72] Auda SH, El-Rasoul SA, Ahmed MM, Osman SK, El-Badry M. *In vitro* release and *in vivo* performance of tolmetin from different topical gel formulations. Int J Pharm Investig. 2015 Jun;45:311–7. doi: 10. 1007/s40005-015-0174-3
- [73] Varma VN, Maheshwari PV, Navya M, Reddy SC, Shivakumar HG, Gowda DV. Calcipotriol delivery into the skin as emulgel for effective permeation. Saudi Pharm J. 2014 Dec;22(6):591–9. doi: 10.1016/ j.jsps.2014.02.007.
- [74] Elsewedy HS, Shehata TM, Soliman WE. Tea tree oil nanoemulsion-based hydrogel vehicle for enhancing topical delivery of neomycin. Life. 2022 Jul;12(7):1011. doi: 10.3390/life12071011.
- [75] Hassan MA, Abd El-Aziz S, Elbadry HM, Samy A, Tamer TM. Prevalence, antimicrobial resistance profile, and characterization of multidrug resistant bacteria from various infected wounds in North Egypt. Saudi J BiolSci. 2022 Apr;29(4):2978–88. doi: 10.1016/j.sjbs.2022.01.015.
- [76] Arafa MG, El-Kased RF, Elmazar MM. Thermoresponsive gels containing gold nanoparticles as smart antibacterial and wound healing agents. Sci Rep. 2018 Sep;8(1):13674. doi: 10.1038/s41598-018-31895-4.